Early Detection of Bladder Cancer Using Autofluorescence, ALA-Induced PpIX Fluorescence and Diffuse Reflectance

Master Thesis
by
Henrik Enquist and Rickard Larne

Lund Reports on Atomic Physics, LRAP-215
Lund, June 1997

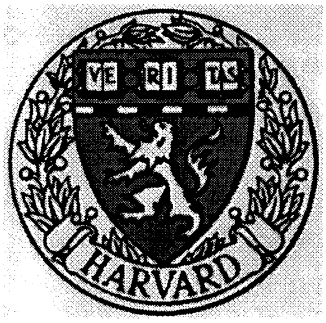

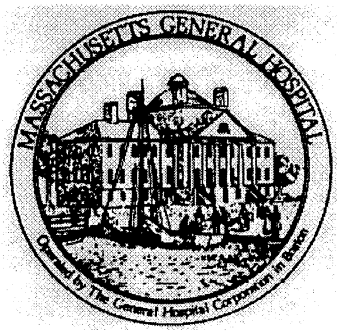

This thesis work was performed at
Wellman Laboratories of Photomedicine at
Massachusetts General Hospital, Boston, USA.
The thesis was submitted to the
Faculty of Technology at
Lund University
in partial fulfilment of the requirements for the degree of
Master of Science.

Abstract

In this study three optical methods, autofluorescence, ALA-induced PpIX fluorescence and diffuse reflectance have been evaluated regarding their ability to detect malignant and dysplastic changes of human bladder tissue, *in vivo*.

For the autofluorescence method, a single-fiber system based on a N_2-laser was used. The 337 nm laser light excited the bladder tissue and the fluorescence was detected with an optical multichannel analyzer (OMA). The differences in the spectra from normal and malignant sites were investigated and the results showed a good demarcation between these tissue types. The sensitivity, specificity and positive and negative predictive values (non-malignant versus malignant) were found to be 73, 90, 73 and 90%, respectively.

The second method utilized 5-aminolevulinic acid (ALA), which has a tendency to predominantly accumulate in malignant tissue. Through the heme cycle the ALA is converted to protoporphyrin IX (PpIX) which fluoresces red when excited with blue light. A filtered xenon-lamp was used to excite the PpIX and the red fluorescence was detected with a CCD camera mounted on a cystoscope. The images were stored on S-VHS tapes and the results were compared with the visual diagnosis made by the surgeon during the procedure as well as with the pathology report, if a biopsy of the site was taken. The easiness with which the PpIX is excited and the fluorescence detected, and the high tumor selectivity of ALA, make ALA-induced PpIX fluorescence a very helpful tool in finding tumors.

The diffuse reflectance method utilized a white light source (xenon-lamp) and an OMA system to record the diffuse reflectance. By comparing the spectral differences between the malignant and non-malignant sites, a quantitative measure of the concentration of hemoglobin was obtained. In practice, this method showed only what was visible to the eye, that the tumor sites appeared red. Though, it provides a quantitative measure and avoids a subjective bias from the surgeon.

Contents

1 Introduction

Optical and spectroscopic methods have proved to be useful in diagnosing various diseases. Since the development of endoscopic instruments and fiber optics, it has been possible to examine the inner organs, such as the gastrointestinal tract and the urine collecting system, using minimally invasive diagnostic procedures. Spectroscopic measurements can improve the diagnosing by giving information about the different types of molecules present in the examined tissue. Also the structure of the tissue is affecting the detected signal, and this makes it sometimes possible to distinguish between different types of tissue.

Bladder cancer is the sixth most common cancer in men and the eighth most common in women. There are over 50 000 new cases reported each year in the USA. After ordinary cystoscopy, there is a recurrence rate of up to 60%. The hypothesis is that small lesions are missed during the standard examination procedure. Small, flat or nodular tumors have a similar appearance to that of normal and inflammatory urothelium. This makes it difficult to detect and diagnose early malignant lesions, including carcinoma *in situ*. The high risk of progression of the lesions, i.e., the increase of the stage and/or the grade of the tumors, makes it even more important to find the tumors at an early stage.

Alternatives to the random biopsy method, which is used as the current standard procedure is desirable. In this study, three optical methods; autofluorescence, ALA-induced PpIX fluorescence and diffuse reflectance have been used trying to detect malignant tissue in human bladders, *in vivo*. The results were compared with pathology results to evaluate the methods. During the standard cystoscopic examination of patients with suspected, treated or recurrent bladder cancer, the optical measurements were performed with the patients consent.

The procedure in the operating room, the cystoscopy, was performed by first filling the bladder with water to keep it distended. Then the cystoscope was put through the urethra into the bladder. During this procedure the patient was under an anaesthetic.

2 Autofluorescence

2.1 Introduction

2.1.1 Basic Theory

When atoms or molecules are electronically excited, by absorption of photons or by another means, there are several ways they can relax. If the system relaxes radiatively between electronic states of identical multiplicity, the emitted light is called fluorescence, see figure 2.1. The wavelength of the fluorescence is longer than the exciting light and it depends on between which energy levels the electron transition occurred.

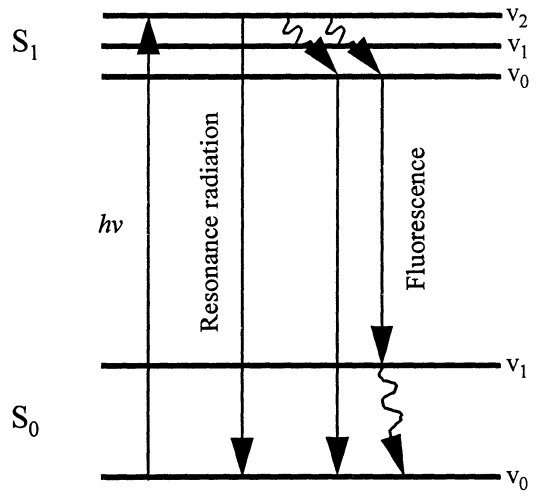

Figure 2.1. Absorption and fluorescence emission.

Figure 2.2 shows a simplified electronic energy level diagram of the levels between which transitions occur. S_0, S_1 and S_2 represent the singlet electronic states and T_1 and T_2 represent the triplet states of a molecule. When a photon is absorbed, depicted by hv_1 and hv_2, the molecule is excited from the ground state, S_0 to an excited state, S_1, S_2 or higher, depending on the wavelength. Photochemical processes may be induced by transitions from S_1 directly or from the first triplet excited state, T_1 after intersystem crossing. The molecule can relax back to S_0 from either S_1, radiatively or non-radiatively (internal conversion) or from T_1 radiatively via a process called phosphorescence. The rate constants for non-radiative decay, radiative decay, intersystem crossing and phosphorescence are represented by k_{nr}, k_r ,k_{isc} and k_p, respectively. In solution, molecules tend to relax via non-radiative means because of the many degrees of freedom. In phosphorescing substances, generally crystals or frozen samples, the S_1 state is depopulated via forbidden $T_1 \leftrightarrow S_0$ transitions and thus an extremely long lifetime of seconds or more is obtained.

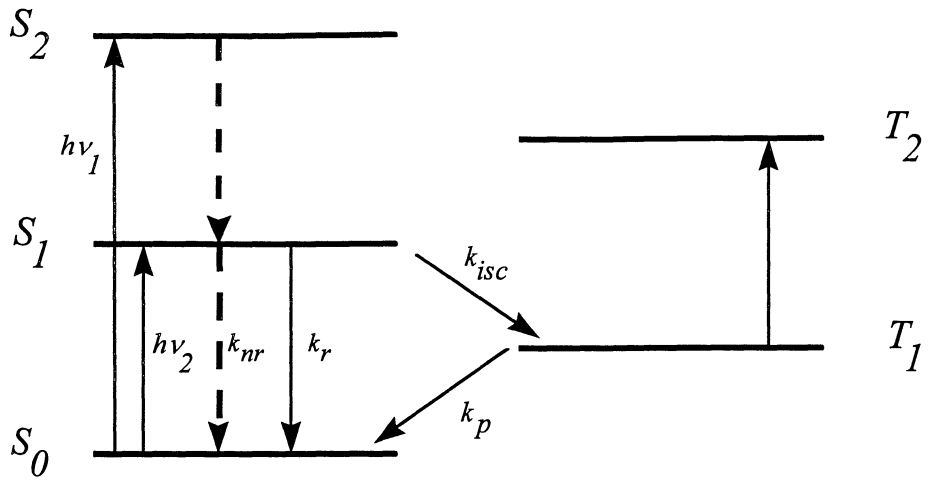

Figure 2.2. Schematic figure of the electronic energy levels of a molecule.

2.1.2 Tissue Autofluorescence

In tissue, autofluorescence is the reemitted light from certain substances and molecules within the tissue when excited by light. The autofluorescence spectrum tends to exhibit broad bands and smooth structures instead of the sharp peaks seen in atomic spectra and this is due to an envelope of vibrational and rotational energy levels of the fluorescent molecules.

Numerous workers have suggested and evaluated the use of tissue autofluorescence as a tool to diagnose diseases in various organs. Presented below is a short overview of some of the different areas where autofluorescence has been used in humans to differentiate between normal tissue and a pathological state, *in vivo* and *in vitro*. Laser-induced fluorescence (LIF) has been shown to be a good method to distinguish atherosclerotic plaque from normal arterial tissue. One of the first studies was performed *in vitro* by Kittrell *et al.* in 1985.[1] This work has been followed by several other groups using different lasers and wavelengths.[2-10] *In vivo* experiments have been performed by Bartorelli *et al.*[11] among others. The results of these experiments have inspired the use of LIF to guide the surgical optics during angioplastic surgery, both for the traditional balloon technique[12-15] as well as for laser ablation of plaque[16-21].

Alfano *et al.* have examined fluorescence from malignant human breast and lung tissue with a good differentiation from normal tissue, though, the number of samples was low.[22] The spectral difference in human teeth using LIF has been studied by at least two groups[23,24] reporting possible discrimination between carious and normal areas.

Andersson-Engels *et al.* have studied the fluorescence of several different types of human organs *in vivo* e.g. brain, lung and ENT (ear, nose and throat) using two wavelengths, 337 and 405 nm.[25] For brain tissue they reported no correlation between spectral differences and various degrees of malignancy. For bronchial tissue there was no difference of the spectral shape of the autofluorescence from malignant lesions compared to normal tissue, whereas for oral/oropharyngeal lesions the malignant areas showed a decreased signal in the violet region (autofluorescence) and an additional peak originating from the endogenous porphyrins. Andersson *et al.*, among others, have studied

autofluorescence from human skin tumor samples[26] and Mahadevan *et al.* have studied cervical lesions[27].

LIF investigations of colonic tissue *in vivo* have been performed by several groups. Two preliminary reports on the use of fluorescence to discriminate normal human colonic mucosa from adenomatous polyps[28] or cancer[29] have shown good results and the work has been continued by other groups[30-33]. Kapadia *et al.* used a HeCd-laser (325 nm) to excite colonic tissue. A six wavelength algorithm was used to identify normal tissue, adenomatous and hyperplastic polyps with accuracies of 100%, 100% and 94%, respectively. Schomacker *et al.* assessed the ability of the technique to distinguish neoplastic from hyperplastic and normal tissue.[30] They used a N_2-laser as excitation source with a wavelength of 337 nm and the fluorescence was recorded with an OMA system. They reported a sensitivity, specificity and positive and negative predictive values toward neoplastic tissue of 80, 92, 82 and 91%, respectively.

To our knowledge five studies have been made on *in vivo* autofluorescence of human bladder tissue.[34-38] Koenig *et al.* have used a 337 nm N_2-laser to excite the tissue and recorded the fluorescence with an OMA. They found that the two major spectral differences between normal urothelium and malignant tumor were a general decrease of the fluorescence intensity for the malignant areas and a missing peak at ~385 nm which was present in the spectra from non-malignant sites, including inflammatory areas. The decrease in the autofluorescence signal was believed to relate to increased light absorption by hemoglobin due to the higher supply of blood in malignant and inflammatory areas. The fluorescence was also believed to be scattered in the hyperplastic urothelium found in tumors. The spectral differences, the missing peak at 385 nm, they have attributed to collagen-associated substances. Since there is no collagen in the urothelium, it was proposed that the fluorescence signal from molecules associated with this chromophore was changed through scattering in the additional transitional cell layers. They have proposed that the decreased signal around 385 nm in tumors could be used as a diagnostic parameter.

Anidjar *et al.* have evaluated different excitation wavelengths (308, 337 and 480 nm) to assess the use of laser-induced autofluorescence diagnosis of bladder lesions. Using the wavelengths 337 and 480 nm they reported the same general intensity decrease for malignant lesions, including carcinoma in situ (Cis), also reported by Koenig *et al.* Both groups have concluded that the overall decrease in intensity for the malignant tumors was independent of grade and stage, see appendix 2, and could be used as a criterion for malignancy. With an excitation wavelength of 308 nm they observed a broad fluorescence band with two secondary maxima at ~360 and 440 nm, respectively, for normal mucosa. The 360 nm peak they attributed to the fluorescence from the amino acid tryptophan. The measured malignant areas lacked the 440 nm peak and the ratio I(360)/I(440) was used to differentiate the malignant areas, including Cis from normal and inflammatory mucosa.

Baert *et al.* have studied the *in vivo* fluorescence from different bladder lesions in 21 patients after injection of Photofrin (a tumor selective photosensitizer, see chapter 3). They used a point monitoring OMA system to detect the fluorescence excited with a Hg-lamp with a filter wheel. The tissue- and photosensitizer fluorescence were studied using two excitation wavelengths, 337 and 405 nm. For the 405 nm excitation, the ratio I(630)/I(500) of the fluorescence was used in the algorithm. In addition to the fluorescence at ~630 nm from the tumor specific sensitizer, the autofluorescence related intensity at ~500 nm was found to be lower for malignant areas than normal, providing potential application as a diagnostic parameter. The results showed a good demarcation

between papillary tumors and normal tissue. Also, certain cases of dysplasia could be differentiated from normal mucosa, whereas some inflamed areas had normal appearing fluorescence spectra (no significance). With 337 nm excitation, four wavelengths were used in the diagnostic algorithm. The purely autofluorescence related I(460)/I(400) ratio was plotted versus the porphyrin related I(630)/I(460) ratio and the demarcation between papillary tumors and normal bladder wall with this algorithm was good.

2.1.3 Bladder Fluorophores and Chromophores

The autofluorescence signal of the bladder wall is considered to depend mostly on the innate tissue fluorophores, reduced nicotinamide adenine dinucleotide (NADH), flavin adenine dinucleotide (FAD), tryptophan and collagen.[34,35,39] Light with wavelengths from 275 to 450 nm overlap the absorption maxima of these fluorophores and is appropriate for excitation; the optimum wavelength for excitation in a fluorescence diagnostic application is not obvious and depends on the fluorescence peaks used in the diagnostic algorithm. In addition, absorption by tissue hemoglobin, which is the main bladder chromophore in the visible spectrum, can change the shape of the fluorescence spectrum via secondary filtering effects.

NADH is primarily located in the metabolically active cell layer of the muscle cells but is also found in the other cell layers. Collagen is predominately located in the lamina propria and the muscle, however, there is no collagen in the urothelium.

With an excitation wavelength of 337 nm, Schomacker *et al.* have reported fluorescence peaks for crystalline NADH and crystalline collagen at ~455 nm and ~394 nm, respectively, see figure 2.3.[32] The wavelengths of the peaks shift *in vivo* compared to *in vitro* because of absorption by hemoglobin, which has a strong absorption band peaking at ~420 nm (the *Soret band*) and a second absorption band (the *Q band*) at ~540-580 nm, see chapter 4. Wavelengths for maximum excitation and emission for some of the bladder fluorophores are presented in table 2.1.

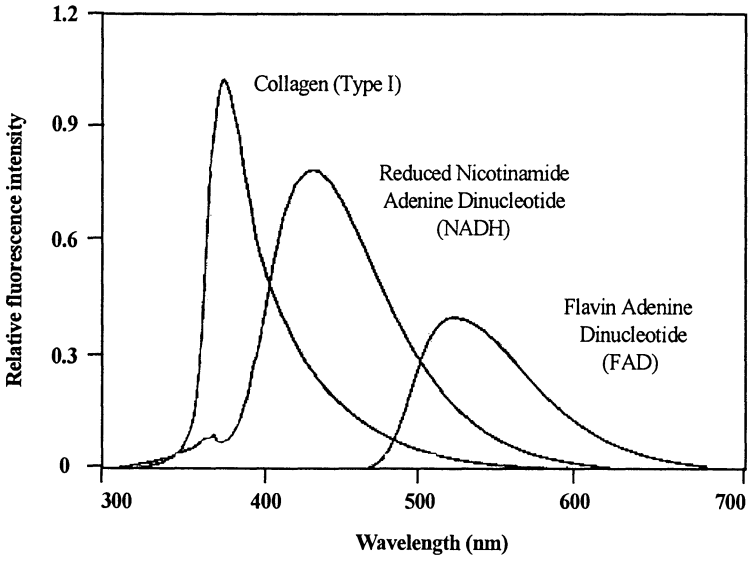

Figure 2.3. Emission spectra for bladder fluorophores (crystalline form) following 337 nm excitation.[32]

Fluorophore	Wavelength (nm)	
	Excitation	Emission
Tryptophan	275	350
Collagen	335	390
NADH	340	450
Oxidized flavins	450	530

Table 2.1 Wavelengths for maximum excitation and emission for common biological fluorophores.[35,40]

For a wavelength of 337 nm, 86 % ($1-e^{-2}$) of the detected fluorescence in colonic tissue was found to originate from within the uppermost 480 μm.[32] It was assumed that the conditions are similar in the bladder wall. Because of this deep penetration it was expected that the recorded fluorescence originates from the underlying lamina propria as well as from the muscle layers, see figure 2.4. Since there is no collagen in the urothelium, Koenig *et al.* proposed that the increased number of transitional cell layers in the malignant lesions could be one of the parameters that caused the lower collagen signal which was reported being typical for the tumors.

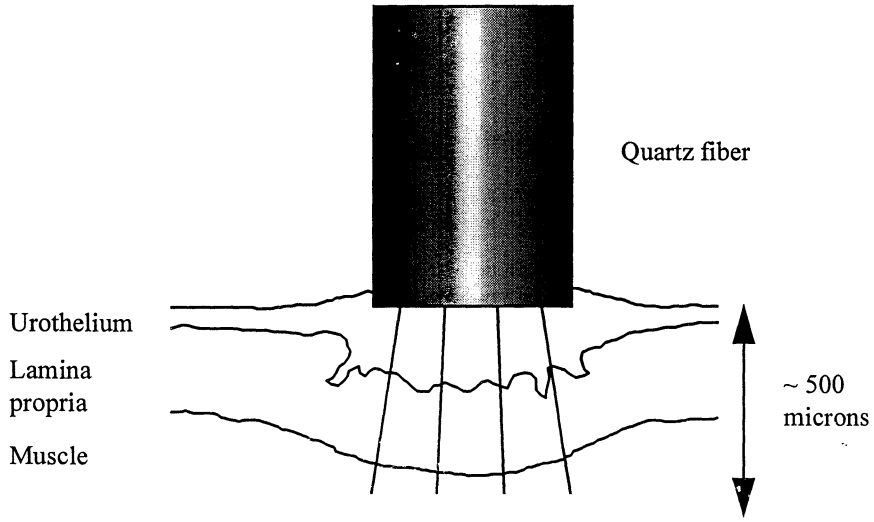

Figure 2.4. Approximate sampling depth of the 337 nm laser light.

2.1.4 Goal

The goal of this study was to further investigate the method proposed by Koenig *et al.*[34] in a prospective study. The ability of an *in vivo* autofluorescence method to diagnose suspicious lesions, such as hypervascularized, edematous and raised, was assessed. The study is thus concentrated on the lesions the urologist could not diagnose during ordinary cystoscopy. The purpose was to try to separate malignant from non-malignant lesions.

2.2 Materials and Methods

The experimental setup is shown in figure 2.5. For the measurements a nitrogen-laser as the excitation source and an OMA system to detect the fluorescence was used. All autofluorescence measurements in this study were done with a single fiber. This equipment made it possible to obtain a complete spectrum for every laser pulse. The sterilized fiber from the OMA system was advanced through a working channel in the cystoscope and placed in contact with the bladder wall when a measurements was made.

2.2.1 Optical Multichannel Analyzer System

Since autofluorescence is very weak, compared to e.g. reflectance, the detector system must have a high sensitivity. To increase the signal an intensifier is placed in front of the diode array. The noise level must also be minimized to allow quantitative measurements and this was achieved by cooling the detector with a Peltier element (reduces the dark current) and by pulsing the excitation source and gating the detector (minimizes the influence of the background light). The short exposure time used for each laser pulse allowed fast averaging of 50 scans for each measurement, which increased the signal-to-noise ratio.

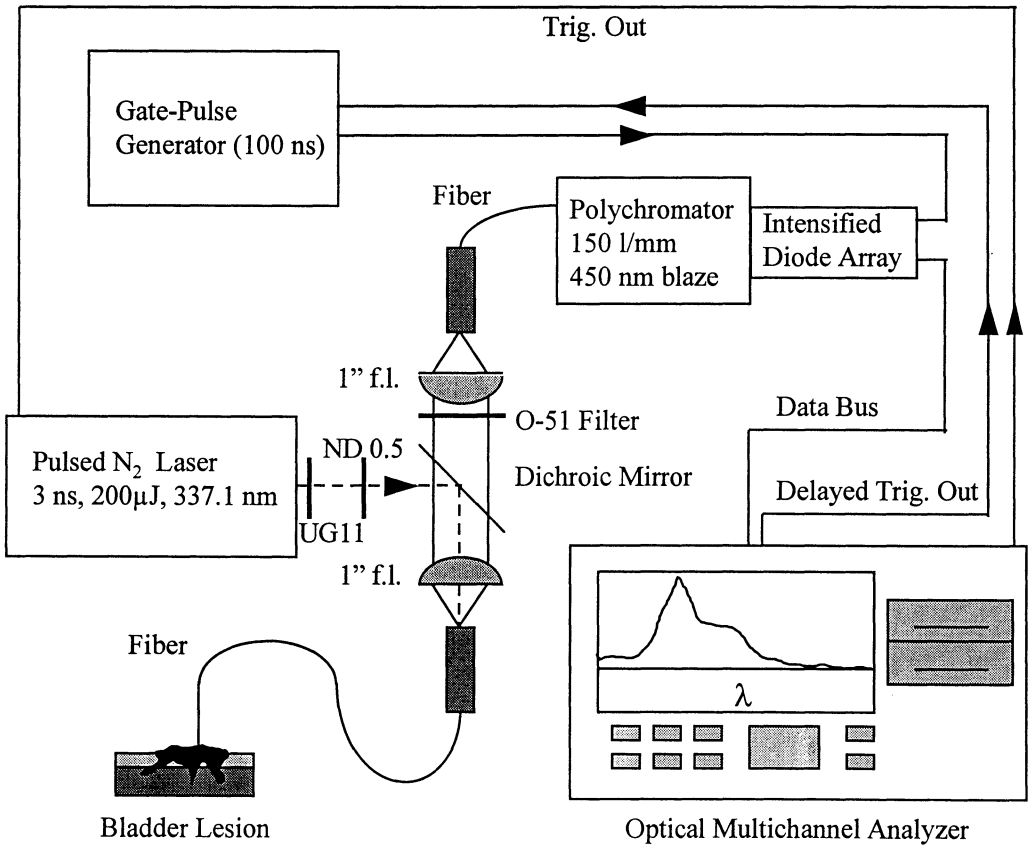

Figure 2.5. Experimental setup.

Quartz fibers and lenses were used due to the short wavelength of the laser light (337 nm). Fibers made of ordinary glass would have attenuated the ultraviolet light and could even have caused fluorescence in the fiber itself.

Tissue fluorescence was excited by light pulses generated by a nitrogen-laser (VSL-337ND, Laser Science Inc., Cambridge, MA). The output of the laser (337.1 nm, 3 ns pulses at 10 Hz and 200 μJ pulse energy) was filtered through two filters, one UG11 and one neutral density 0.5, through a quartz lens into an optical fiber (quartz, 600 μm core diameter). Typical energies delivered to tissue were approximately 40 μJ/pulse. The fluorescence emitted from the tissue was transmitted via the same optical fiber and optically coupled into a 0.275-m polychromator (Monospec 27, Anaspec, Acton, MA). A SMA fiber optic connector was used to couple the sterile fiber to the measuring system. The fluorescence spectra (300-800 nm) were recorded using an intensified 1024-diode array optical multichannel analyzer system (OMA III, Princeton Applied Research, Princeton, NJ), which displayed the spectrum in 0.6 nm increments. The grating had 150 lines/mm and a 24 nm/mm dispersion and was mounted for 450 nm blaze, see figure 2.6. The spectral resolution of the OMA system depends on the number of diodes in the array and by the grating used.

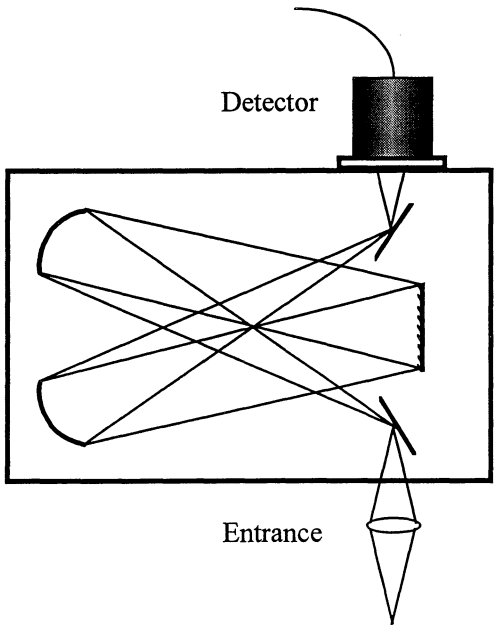

Figure 2.6. Sketch of the spectrograph (crossed Czerny-Turner).

The intensifier was gated with 100 ns pulses centered on the 3 ns laser pulses. It consisted of three parts, a photocathode, a microchannel plate (MCP) and a phosphor screen, see figure 2.7. When light with enough photon energy impinges on the photocathode, it releases one electron per photon, according to the photoelectric effect. The electrons are then accelerated by an electric field in the MCP. The MCP is in fact many small parallel, spatially arranged tubes which are covered on the inside with a material emitting secondary electrons. The phosphor screen converts the final electron shower back to light, which is detected by the diode array. With this technique, an amplification of more than 10^4 can be achieved.

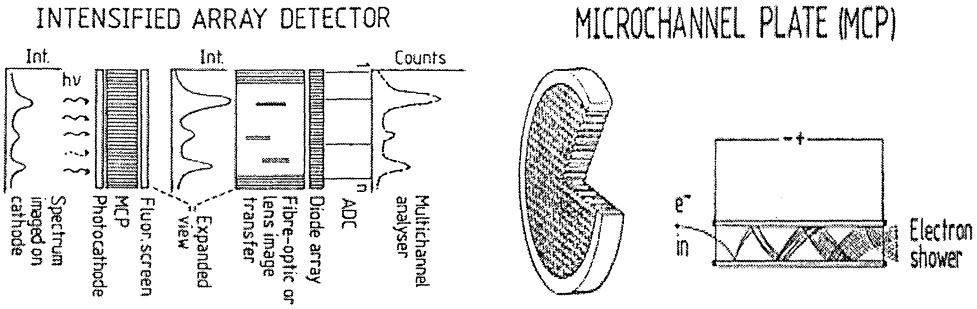

Figure 2.7. Intensified diode array with a microchannel plate.[41]

2.2.2 System Calibration

The diode array was initially calibrated spectrally using a low-pressure mercury-lamp (model 6035, Oriel Corp., Stratford, CT), see appendix 3. The spectrometer calibration was checked before every *in vivo* measurement using the 435.8 nm line of the fluorescent light tubes in the operating room. Variations in laser energy and fiber coupling efficiencies were taken into account by measuring the fluorescence from a cuvette of laser dye (DCM, Exciton Inc., Dayton, OH) of known concentration directly after the autofluorescence measurements.

2.3 Measurement Technique

The urologist first performed the standard cystoscopical procedure, visually inspecting the bladder wall thoroughly to detect nodular tumors as well as suspicious lesions (hypervascularized, edematous, raised and so forth). If a suspicious area was found and a biopsy was to be taken, the fiber was advanced through a working channel in the cystoscope. The fiber tip was gently placed on that location and a spectrum was recorded. After that, the biopsy was taken from the same spot using a pair of forceps. The data were analyzed off line and correlated with the histology report, independently. To minimize the possible interobserver variability the measurements were performed by only two urologists (82 and 18% of the patients respectively).

Measurements were made on different types of lesions. Data was obtained from normal appearing urothelium as well as from suspicious sites. Also random areas were measured according to a standard protocol which was required for some of the patients. These sites could have appeared red and inflamed due to previous bladder cancer treatment or could have looked normal to the surgeon.

Due to clinical importance, it was decided to concentrate the study on only the suspicious bladder areas. This approach was chosen because these lesions are difficult to diagnose during the cystoscopic procedure. The papillary tumors are usually visible and it is well known that over 95% of these tumors are malignant. It is thus more important to find alternative methods for detection and diagnosis of flat lesions.

Measurements were performed on 26 patients of which 22 (14 male and 8 female) were eligible for the study. The median age of these patients was 72 years. The remaining 4 patients were included in the study of autofluorescence from papillary tumors, which is discussed later.

Fortytwo biopsies were taken and the average number of biopsies per patient was 1.9 (range 1 to 5). According to the histological results, data was obtained from several types of lesions including normal urothelium, dysplastic lesions, micro-papillary and nodular transitional cell carcinoma, carcinoma *in situ*, calcified/necrotic tissue and areas with chronic cystitis (inflammation of the bladder) or cystitis glandularis, see table 2.2. In addition to the suspicious lesions, measurements were also made on papillary transitional cell carcinomas (27 sites) and squamous papillomas (3 sites) and the results were confirmed by histological reports. The results from these tumors are not included in the study, but are discussed later. Also the calcified/necrotic lesions measured (2 sites) were excluded because of the nature of the tissue (i.e. necrotic) and the non-biological properties of the calcified areas.

Bladder lesions			
Cystoscopical appearance	Number of sites	Histological report	Number of sites
Normal	12	Normal	6
		Chronic Cystitis	2
		Cystitis Glandularis	3
		Dysplastic	1
Suspicious	30	Normal	3
		Chronic Cystitis	11
		Dysplastic	5
		Carcinoma *in situ*	6
		Transitional Cell- TaG1	1
		Carcinoma T2G3	4
Number of sites	42		42

Table 2.2. Histology of suspicious bladder areas.

2.4 Results

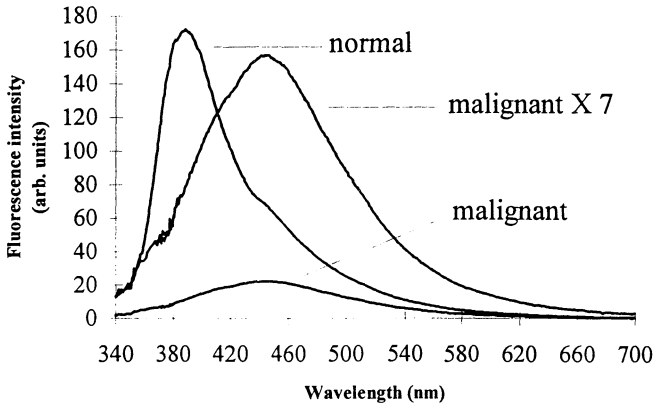

Figure 2.8. Typical autofluorescence spectra for normal and malignant tissue (from the same patient).

The two most prominent differences between malignant and normal urothelium were found to be the lower total integrated fluorescence intensity and the lack of the peak around 391 nm in the malignant spectra. The 391 nm wavelength is the calculated average peak wavelength for the spectra from the normal sites.

In figure 2.8 typical spectra are shown for normal and malignant bladder tissue. As can be seen, there is a wavelength shift of the peak from 391 nm to 455 nm in malignant lesions. The inflammatory lesions typically show both the peak at 391 and the broader peak (band) around 455 nm, see figure 2.10. The 455 nm band can also be seen as a small shoulder in the spectra from normal tissue.

Bladder areas	**I(391)/I(455) ratio**			**Number of sites**
Histology	**< 1.20**	**> 1.20**	**Mean +/- SD**	
Transitional Cell Ca	5	0	0.88 +/- 0.16	5
Carcinoma *in situ*	3	3	1.17 +/- 0.62	6
Dysplasia	2	4	1.83 +/- 1.20	6
Cystitis	0	13	2.03 +/- 0.84	13
Cystitis Glandularis	1	2	2.07 +/- 1.26	3
Normal urothelium	0	9	1.73 +/- 0.38	9
Number of sites	11	31	-	42

Table 2.3. I(391)/I(455) fluorescence ratio.

A ratio of the fluorescence intensity was calculated using the wavelengths 391 and 455 nm. The data are presented in table 2.3. Also the integrated fluorescence intensity was calculated, see table 2.4. A combined scatter plot of these two parameters is shown in figure 2.9. Using both the ratio and the integrated fluorescence intensity in the diagnosis increased the accuracy of the method compared to if only a single parameter was used.

Bladder areas	**Integrated fluorescence intensity**	**Number of sites**
Histology	**Mean +/- SD**	
Transitional Cell Carcinoma	0.28 +/- 0.11	5
Carcinoma *in situ*	0.70 +/- 0.54	6
Dysplasia	1.31 +/- 0.91	6
Cystitis	1.31 +/- 0.79	13
Cystitis Glandularis	1.04 +/- 1.03	3
Normal urothelium	1.01 +/- 0.48	9
Number of sites		42

Table 2.4. Integrated fluorescence intensity.

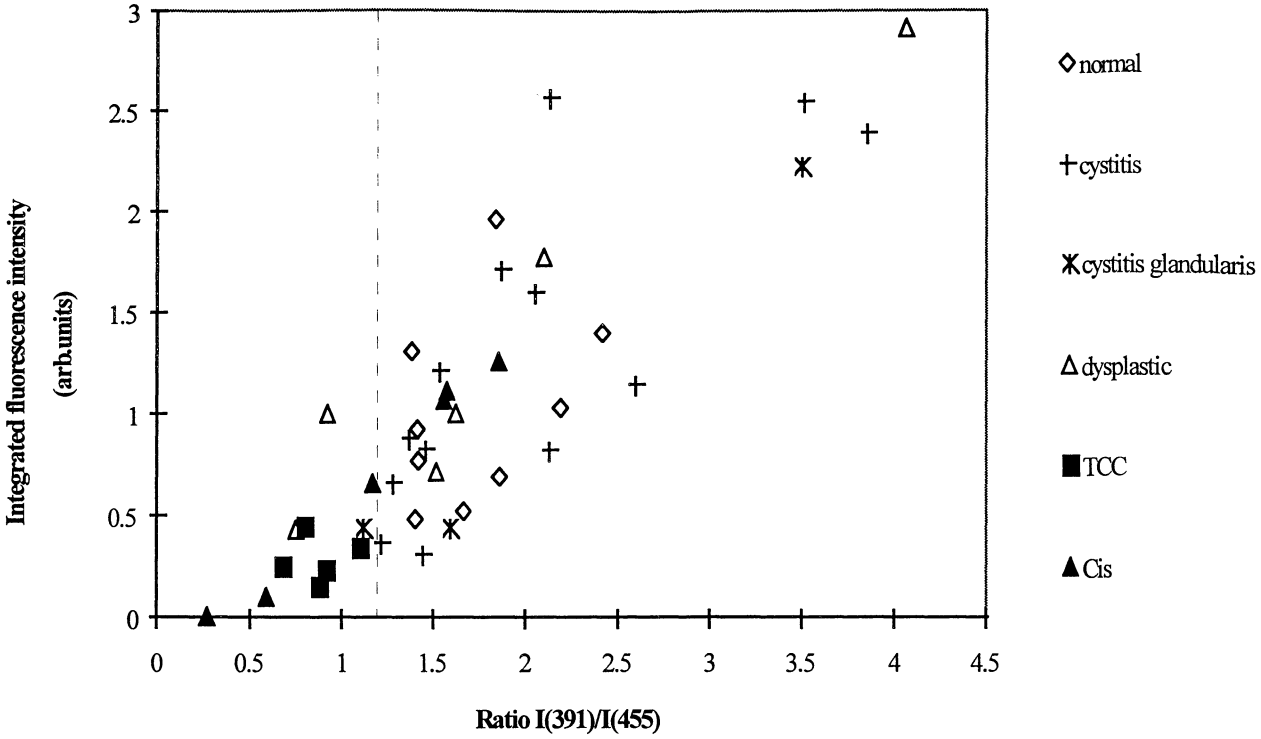

Figure 2.9. Integrated fluorescence intensity vs. I(391):I(455) ratio with the 1.20 threshold.

The I(391)/I(455) ratio 1.20 was chosen as the separation criterion for malignancy and the threshold line is shown in figure 2.9. For this given value, the sensitivity, specificity and positive and negative predictive values were calculated for two different groups of lesions, malignant vs. non-malignant as well as for malignant and dysplastic vs. normal and cystitis. The results are presented in table 2.5. To include the dysplastic lesions in test group 2 could be clinically correct because of the fact that dysplasia in the bladder is considered to be pre-malignant and such lesions are resected if found. The difference between dysplasia and a malignant tumor is sometimes very small. The difference could be a matter of the extent of hyperplasia. On a cellular level, the dysplastic and the malignant lesion could appear identical.

	Group 1: Malignant	**Group 2: Malignant and dysplastic**
Sensitivity	73 %	59 %
Specificity	90 %	96 %
Positive predictive value	73 %	91 %
Negative predictive value	90 %	77 %

Group 1: $p<0.003$ compared to non-malignant
Group 2: $p<0.027$ compared to normal and cystitis
Student's t-test

Table 2.5. Results.

In figure 2.10, different areas histologically determined to be inflamed are plotted. Mild cystitis has a spectrum which is similar to that of normal tissue, whereas

moderate cystitis has a lower overall intensity. The spectra from inflamed areas have a non-malignant shape and display both the 391 and 455 nm peaks.

Two of the cystitis and 2 of the cystitis glandularis specimens came from patients that had undergone past treatment for bladder cancer (chemotheraphy, radiation) which may lead to acute or chronic inflammation of the bladder.

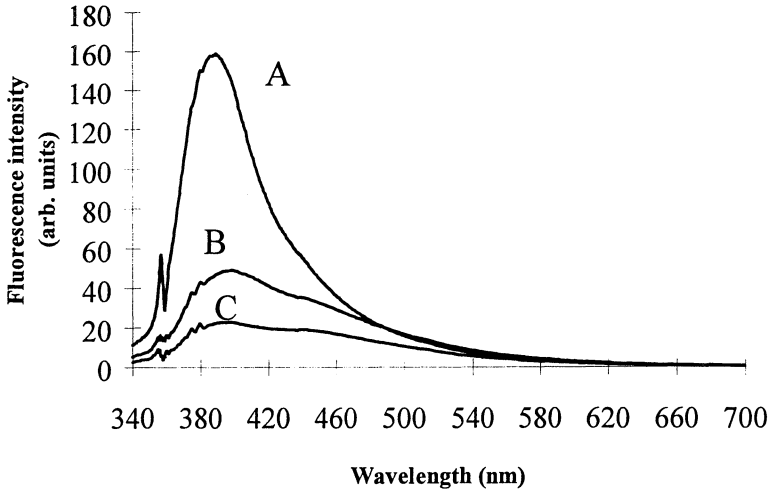

Figure 2.10. A: Mild chronic cystitis, B and C: Moderate chronic cystitis (from the same patient).

Two of the dysplastic sites were classified as malignant by this method (moderate dysplasia). Three of the Cis tumors measured had a tumor typical fluorescence ratio (<1.20). Some spectra from Cis lesions are shown in figure 2.11.

2.4.1 Thickness Measurements

To get an idea of the thickness of the detected lesions, the urothelium of some of the specimens was measured from the pathology slides using a microscope with a built-in scale. The thickest and the thinnest areas of the urothelium were measured for each specimen, see table 2.6.

There was always an uncertainty of where the fiber was placed on the lesion, on a thicker part or a thinner, so it cannot be determined which of these two values is the most relevant. A fair conclusion is that the true thickness of the urothelium at the measurement site should have a value somewhere between the maximum and minimum thickness measured from the pathology slide. It is then assumed that the biopsy was taken from the same spot as the fluorescence measurement. The detection limit for malignancy seemed to be a urothelial thickness of ~150-200 μm, which is a doubled number of cell layers compared to normal.

Bladder lesions Histology	Urothelium thickness (μm)		Fluorescence ratio I(391)/I(455)
	max	min	
Normal Urothelium	38	0	2.19
	50	13	1.38
	75	50	1.86
Carcinoma *in situ*	150	38	1.17
	300	25	0.27
	300	25	0.59
	700	50	1.57
	1000	(0)	1.85
Micro-papillary TCC	200	25	0.92
	200	63	0.80
Dysplasia	125	(0)	4.06
	125	25	1.62
	175	25	2.10
	200	25	0.92
	200	25	0.75
Squamous Papilloma	1250	380	1.16
	1250	380	0.94
Papillary TCC	250	50	1.82
	500	75	2.38
	700	50	1.41
	1000	50	0.33
	1000	50	0.66
	1000	50	0.27
	1750	200	0.54
	5000	3500	1.09

Table 2.6. Urothelium thickness of different lesions measured from pathology slides.

2.5 Discussion

The results correspond well to the results reported by Koenig *et al.* This group reported a sensitivity, specificity and positive and negative predictive values of 97, 98, 93 and 99%, respectively. They have included papillary tumors as well as suspicious flat lesions, which is not done in this investigation. Another difference is that they used the wavelength 385 nm in their algorithm to represent the collagen signal. The data from this study show an average peak at ~391 nm, which is the wavelength used in this study. This wavelength lies between the 394 nm wavelength for crystalline collagen reported by Schomacker *et al.*[30] and the 390 nm reported by Anidjar *et al.*[35] The difference in wavelength between crystalline collagen and collagen *in vivo* could be explained by scattering effects and blood absorption in the *in vivo* case, but also by the polarity and the pH of the environment.

Koenig *et al.* also used a different threshold for malignancy (1.01 compared to the value of 1.20 in this study). This difference is most likely due to a systematic instrumental effect and in particular to how the instrument is corrected for spectral sensitivity (system response). Although the same setup was used as in the Koenig *et al.* study, a different system response curve was obtained, which could explain the wavelength differences.

The results of this study show a lower sensitivity and selectivity than those reported by Koenig *et al.* This could be explained by the higher number of Cis lesions

included in this study. Six sites with Cis were measured (20% of all suspicious sites) compared to 1 in their report (2%). Cystoscopically, Cis can appear similar to acute or chronic cystitis, or even mimic normal mucosa. This makes it very difficult for the urologist to determine whether the area is malignant or not. This was the only type of malignant lesions that were diagnosed as non-malignant (false-negative, 3 areas). All other malignant tumors (nodular and micro-papillary) were correctly diagnosed. Cis lesions exfoliate transitional cells at a high rate,[42] which leads to a thinner urothelium (0-3 layers of cells) in some Cis lesions and this could increase the collagen signal, see figure 2.10.

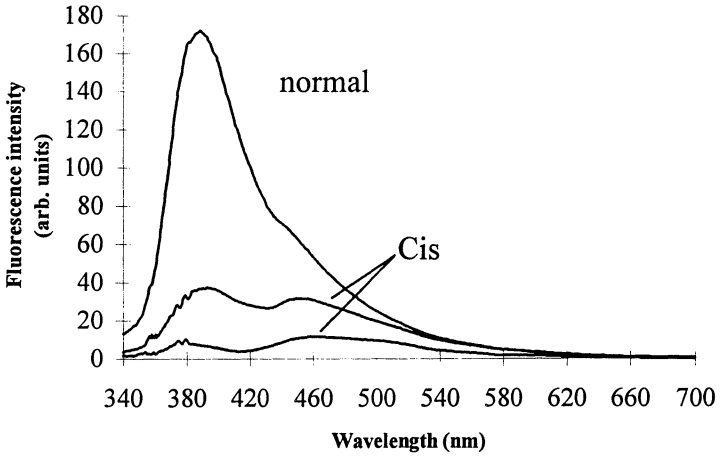

Figure 2.11. Spectra from normal tissue and two Cis lesions classified as malignant (from the same patient).

This supports the hypothesis that it is the urothelium thickness that is indirectly measured. As can be seen in table 2.6, Cis lesions have areas with thicker urothelium compared to non-malignant sites, but also areas with only a couple of, or even no, cell layers. It is impossible to know where the fiber was placed on the lesion and the fluorescence result could be negative if the fiber was placed on a thinner area. The fifth Cis lesion listed in table 2.6 was focal with surrounding partly denuded urothelium. It was thus not surprising that this site was detected as negative because of the difficulty in placing the relatively thick fiber (600 μm) on the small malignant spot (50-80 μm). On the other hand, if the tumor is wider, as in the case of the second and third Cis sites listed in table 2.6, it was more likely for the fiber to hit the tumor and as a result, the fluorescence signal was positive.

Two of the dysplastic lesions were detected as malignant. This could be explained by the fact that dysplastic lesions are sometimes hyperplastic and hence have an increased number of urothelial cell layers. This hypothesis is supported by the results showed in table 2.6. The two detected dysplastic lesions had a maximum thickness of 200 μm, which is more than double the normal thickness. Dysplastic lesions in the bladder are considered to be pre-malignant and will be resected if found.

The lower overall fluorescence intensity found in some inflammatory areas could be explained by increased blood absorption of the exciting and fluorescence light. The absorption depends on the amount of blood in the tissue. However, since the inflammations were not always graded in the histology report (mild, moderate or extensive), this absorption effect could not be estimated for each site measured. Only one

measured inflamed area (cystitis glandularis) was diagnosed as malignant (false positive) with this method. It is shown in chapter 4 that malignant lesions have a higher amount of blood than normal tissue, but this is also true for the inflamed areas which appear red but do not have positive spectra. This suggests that it is not only light absorption in hemoglobin that gives the fluorescence from the malignant areas their typical spectral shape. An explanation for the false positive cystitis site could be that there was a high number of lymphocytes in the upper layer of the lamina propria. These cells could have scattered and absorbed the fluorescence. The cystitis glandularis also had a thickening of the urothelium and hence showed a tumor like structure.

The two calcified necrotic areas measured had ratios below the demarcation limit of 1.20 as well as a low integrated intensity, mimicking the spectrum of malignant tissue. This could be explained by higher scattering and absorption of the excitation and emission light by the calcification or by the lack of collagen in this type of lesion. Since the necrotic tissue, as well as the calcifications, does not have the same fluorescence properties as living tissue, normal signals from these areas were not expected. The fact that positive signals from this kind of lesion were obtained only strengthens the theory that it is the increased thickness of the urothelium, and hence a lower collagen signal, that is measured with this method.

The results for the papillary tumors measured were more varied. Two of the spectra obtained are shown in figure 2.12. As can be seen, curve A is very similar to a spectrum from normal tissue whereas curve B has the same features as the spectra measured from the flat malignant lesions included in the study. The detection of the fluorescence light could depend on the position of the fiber on the papillary tumor. The structure of a papillary lesion is inhomogenous with areas where the thickness of the urothelium is close to normal and from such an area the collagen signal is high, giving a false negative result. As seen in table 2.6, all of the very large and thick papillary tumors were detected.

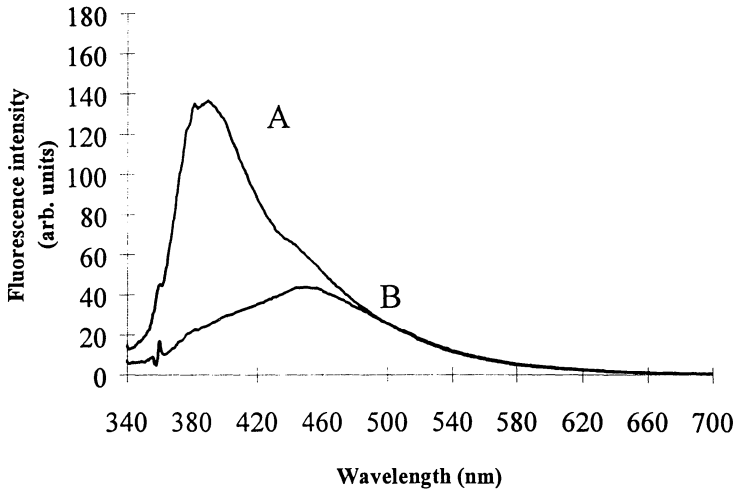

Figure 2.12. Two spectra from the same papillary tumor.

For some of the other smaller papillary tumors the fiber could have been placed on an area with a thickness close to normal, giving a false negative collagen signal originating from the lamina propria. Papillary tumors are also sensitive to pressure and

easily bleed even when gentle contact pressure is applied. Blood has a broad absorption band caused by oxy- and deoxyhemoglobin between 300 and 600 nm, with a peak at the *Soret band* at ~420 nm, see chapter 4. The absorption of the fluorescence light is stronger at 455 nm than at 391 nm which could lead to a change in the I(391)/I(455) ratio. This hemoglobin absorption effect and the fiber placement difficulty could explain the false negatives encountered when measuring papillary tumors.

Two squamous papillomas were measured (data not presented). These were thick papillary structures of squamous cells instead of transitional cells and were diagnosed as malignant with fluorescence ratios lower than the threshold value 1.20. This, in addition to the fact that all nodular and micro-papillary transitional cell carcinomas, independent of grade, were detected, suggests that the tumor structure and morphology are major causes for the differences of the fluorescence spectra between malignant and non-malignant sites rather than fluorophore changes due to the tumor metabolism.

The results presented here show that it is not certain that it is only a thickening of the urothelium that gives the malignant sites their typical spectral shape. It is most probably a combination of this scattering effect and absorption in hemoglobin. An attractive feature of the autofluorescence method is that it utilizes natural properties of the cancerous tissue, i.e. the increase in thickness of the urothelium and an increased amount of blood. This is a direct and thus desirable way of detecting cancer and it does not depend on the use of exogenous drugs. A disadvantage of this method is that only a single point is examined at each time. The autofluorescence point measurement method could be combined with the ALA-induced PpIX fluorescence method, which provides a tumor detecting image of the bladder. The autofluorescence method could then serve as an optical biopsy technique *in vivo*. If an autofluorescence imaging system is constructed, it would be possible to scan the whole area of the bladder wall and at least one group is developing such a system.[35] The use of an imaging technique would eliminate the problems associated with the fiber-tissue contact (bleeding, compression or penetration of the urothelium etc.) and would provide an image, which is always preferred by surgeons. Autofluorescence imaging has been used in a couple of clinical studies of human tissue (e.g. colon and lung) and the published results are encouraging.[43-45]

2.6 Conclusions

Laser-induced tissue autofluorescence has proven to be a useful diagnostic tool in many types of human tissue *in vivo* and *in vitro*. This study showed that using the autofluorescence of bladder tissue, excited by a N_2-laser, it was possible to distinguish malignant and some dysplastic lesions from non-malignant and inflammatory tissue. The study was focused on suspicious areas that the urologist could not diagnose by eye during the standard cystoscopical procedure. Detection and correct diagnosis of flat suspicious lesions at an early stage is especially important because early detection increases the chance of a successful treatment and lowers the recurrence rate.

This autofluorescence method could be used *in vivo* to diagnose suspicious lesions, minimizing the number of biopsies and presenting immediate diagnosis. A major disadvantage is that 3 of 6 lesions with carcinoma *in situ* were missed. Some advantages with this method are that 36 of 42 areas, including all 5 micro-papillary tumors, were

correctly classified and that 27 of 30 benign lesions would have been saved from biopsy if the fluorescence results were used during the procedure.

3 ALA-Induced PpIX Fluorescence

3.1 Introduction

Exogenous fluorescent tumor markers (substances that preferentially accumulate in tumors) can be delivered in concentrations that lead to higher fluorescence contrast between tumors and the surrounding tissue than autofluorescence, and thus, to simpler detection of tumors. However the question with any tumor marker is how specific it is in marking tumor versus normal tissue.

Using a fluorescent tumor marker has the advantage of giving control over the excitation and emission wavelengths. In comparison with autofluorescence this is a major advantage. This makes it possible to choose a tumor marker that fluoresces in the wavelength region where the absorption from the surrounding tissue is low, and consequently, does not absorb much of the fluorescence. Also, low absorption implies low background fluorescence. Drawbacks with using a tumor marker is the additional invasive procedure, e.g. if the tumor marker is given intravenously or through instillation, and the additional drug involved, compared to autofluorescence measurements.

For diagnosis of tumors, the fluorescence properties of the tumor marker is used. In many cases the tumor marker can also be used for treatment of the tumor, with photodynamic therapy (PDT)[1-4]. This is a photochemical reaction promoting tissue oxidation. The PDT treatment modality is under development. In this thesis a tumor marker used for PDT is referred to as a photosensitizer.

The most common class of tumor seeking substances used for laser induced fluorescence today is hematoporphyrin derivatives (HpD) and related substances.[5-12] One form of HpD is available commercially under the trade name Photofrin (Pf). Clinical results with Pf have been promising and this photosensitizer has received regulatory approval in a number of countries for diagnosing and treatment of cancer. However, it is plagued by prolonged cutaneous phototoxicity, which can last up to 4 to 6 weeks. The selective uptake and retention of porphyrins in tumor tissue has been demonstrated in many investigations.[13] The highest difference in retention between tumors and healthy tissues is found in some brain tumors, attributed to a tight normal brain-to-blood barrier in contrast to a leaky barrier in tumors. In most cases the retention difference has a value between 2:1 and 3:1.[5]

Stability and purification of the different hematoporphyrin related substances are still problems, and one reason for the search for new tumor seeking drugs. Other reasons are the possibility of finding drugs with higher selective accumulation in tumors, higher absorption of the excitation light, higher fluorescence yield and lower skin photosensitivity.

Recently there has been much interest in administering 5-aminolevulinic acid (ALA)[14], which is part of the heme cycle and precursor of the photosensitizer protoporphyrin IX (PpIX). Preclinical studies of diagnosis and treatment in a variety of systems with ALA-induced PpIX have been promising *in vitro*[15] and in animal tumor models[16-18].

Some of the motivation for using ALA-induced PpIX lies in the brief cutaneous photosensitization (less than 24 hours following systemic ALA administration). For diagnosis and treatment involving the urinary bladder, ALA can be given orally, through intravenous injection, or more recently, through instillation in the bladder. Intravesical

application has the advantage of preventing skin phototoxicity since the basement membrane of the urothelium acts as a diffusion barrier for ALA.[19]

By giving the patient ALA, it is possible to detect the red PpIX fluorescence with the naked eye, or using a charged coupled device (CCD) camera. The CCD cameras are relatively inexpensive and can be coupled to a computer via a frame grabber board. This camera, when coupled to a cystoscope, enables imaging of the interior of the bladder without contact and makes it possible to detect areas that might be malignant. Not only malignant areas appear red, but also some inflammatory regions. Even for easily visible tumors, ALA-induced PpIX fluorescence can be useful to tell if the physician has removed the whole malignant area. If not, red fluorescent areas will still be found when the tissue is excited with blue light.

Trials with ALA-induced PpIX fluorescence for diagnosis of early bladder cancer were first described by Baumgartner *et al.* in 1993.[20] They performed the intravesical instillation in 56 patients using a pH-neutral ALA-solution. After two to four hours incubation time they found strong red fluorescence even from early stage urothelial diseases. Kriegmair *et al.* reported a study of 68 patients with bladder cancer in 1994.[21] A krypton ion laser (406.7 nm) was used for excitation and the PpIX fluorescence at 630 nm was studied. They reported a sensitivity of 100% and a specificity of 68.5%. Another investigation, also by Kriegmair *at al.*, was reported in 1996.[22] Here they investigated 104 patients with a suspicion of primary or recurrent bladder cancer. The krypton ion laser was used here as well. The investigation was conducted to determine whether the sensitivity of detecting dysplasia or early bladder cancer could be improved by ALA-induced PpIX fluorescence. They found a sensitivity for blue light cystoscopy of 96.9% in comparison to 72.7% for white light.

The present experiments are part of the first human trials in the USA using ALA for detection of bladder carcinoma.

3.2 Theory of ALA-Induced PpIX Fluorescence

3.2.1 The Heme Cycle

ALA is a naturally occurring precursor in the heme biosynthetic pathway. When ALA is exogenously administered, the feedback control via the enzyme ALA-synthase (ALAS), which prevents too much heme from being produced, is bypassed and ALA can be metabolized to PpIX in large excess, see figure 3.1. PpIX is a photosensitizing and fluorescent species, while ALA is not. The last step in the biosynthetic route is to incorporate an iron ion into the PpIX molecule to form heme. Following exogenous ALA-instillation, PpIX accumulates in the tissue and can be exploited for fluorescence measurements or PDT. Interestingly, when PpIX is administered directly, there is no accumulation in most tumor cells.[23]

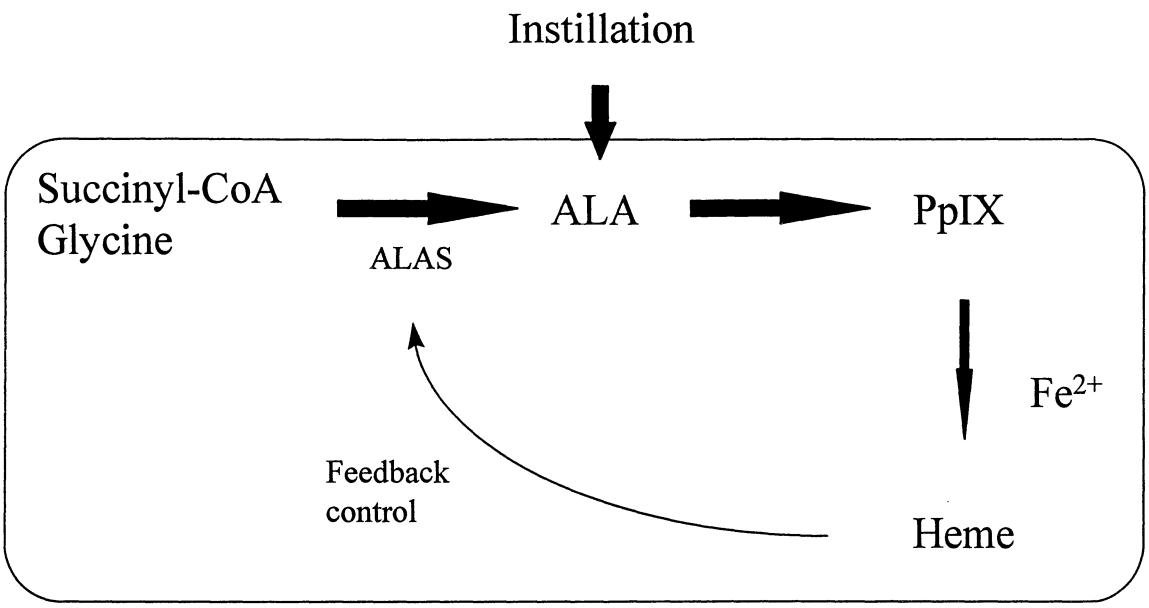

Figure 3.1. The heme cycle. Succinyl-CoA and Glycine form ALA which induces intracellular accumulation of PpIX. PpIX transforms to heme by incorporating an iron ion into the molecule. When too much heme is being produced, the feedback control via the enzyme ALA-synthase (ALAS) prevents more ALA from being produced. By instillation of ALA into the bladder, the feedback control is bypassed, and more PpIX can be produced and accumulated in the cells since the conversion from PpIX to heme is a rate limiting step.

3.2.2 Accumulation of PpIX In Malignant Tumors

The high accumulation of a photosensitizer in neoplastic tissue relative to normal tissue depends on the photosensitizer and the tissue being considered. Why PpIX is preferentially accumulated in malignant tissues compared to normal is not clearly understood, but there are some suggestions. It could be that there is a higher ALA-uptake in the tumor than in normal tissue, for instance when the ALA is being topically administered to basal cell carcinoma (BCC).[24] In that case the compromised stratum corneum of the skin allows more penetration at the site of the BCC. Another explanation would be that more ALA transforms to PpIX in tumor cells.[24] The transformation from ALA to PpIX is made in several steps involving different enzymes. It has been suggested that a higher concentration or activity of one or several of these enzymes in tumor cells, lead to a greater amount of ALA being transferred to PpIX per unit time.[24-26] Since the transformation from PpIX to heme is a rate limiting step, this results in a higher concentration of PpIX in tumor cells. It could also be that cancer cells have a higher capacity of retaining PpIX.[24] The next possibility would be that the higher metabolism of rapidly proliferating tumor cells leads to a more rapid conversion of ALA.[24] Further, another explanation for the stronger fluorescence from tumors than from healthy tissue could be that tumors consists of more cell layers. This means that fluorescence from many layers add up and give a stronger signal.

The accumulation of PpIX in malignant tumors is a topic of active studies, that might help to clarify the phenomenon.

3.2.3 PpIX Fluorescence

PpIX has characteristic absorption spectra in the ultraviolet and visible regions. There is one absorption band around 280 nm, called the *γ-band*, one band around 420 nm, called the *Soret band*, and four bands in the visible region above 500 nm, called the *Q-bands*.[27] When PpIX is excited in the *Soret band* with blue light the fluorescence is detected around 635 nm, see figure 3.2.

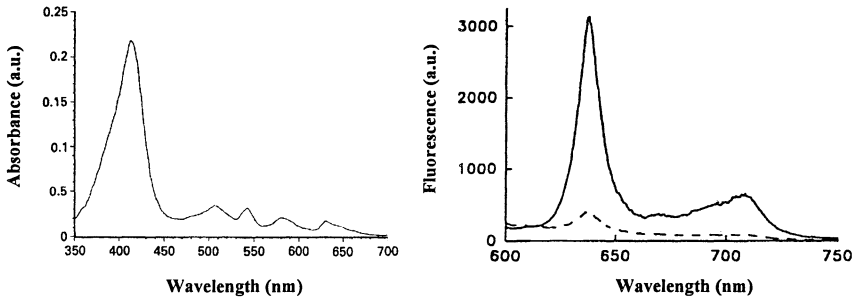

Figure 3.2. Absorption spectrum of PpIX in a cell suspension. NBT-II cells were incubated with 1 mM ALA for 24 h.[15] Fluorescence spectrum of ALA-induced PpIX in normal mucosa (dashed line) and papillary bladder cancer, TaG2 (solid line), excited with a krypton ion laser (406.7 nm).[21]

3.3 Materials and Methods

3.3.1 Patients

Fluorescence measurements were performed in 16 patients with bladder cancer undergoing mucosal biopsies or transurethral resection of the bladder at initial diagnosis or at regular bladder tumor follow up visits. Average patient age was 67 years (range 39 to 83 years).

3.3.2 ALA Instillation

Cystoscopy was performed 2 to 3 hours after intravesical instillation of 50 ml of a freshly prepared ALA solution (1.5 g 5-ALA hydrochloride dissolved in 1.4% $NaHCO_3$, pH 5) in 19 patients with a suspicion of primary or recurrent bladder cancer. In 3 of these patients no biopsies were taken and these results are not included. The time was chosen on the basis of the experiences of other groups and reflects the optimal time needed for enough ALA to be taken up by the cells and transformed into the fluorescent PpIX.[22]

3.3.3 Light Source

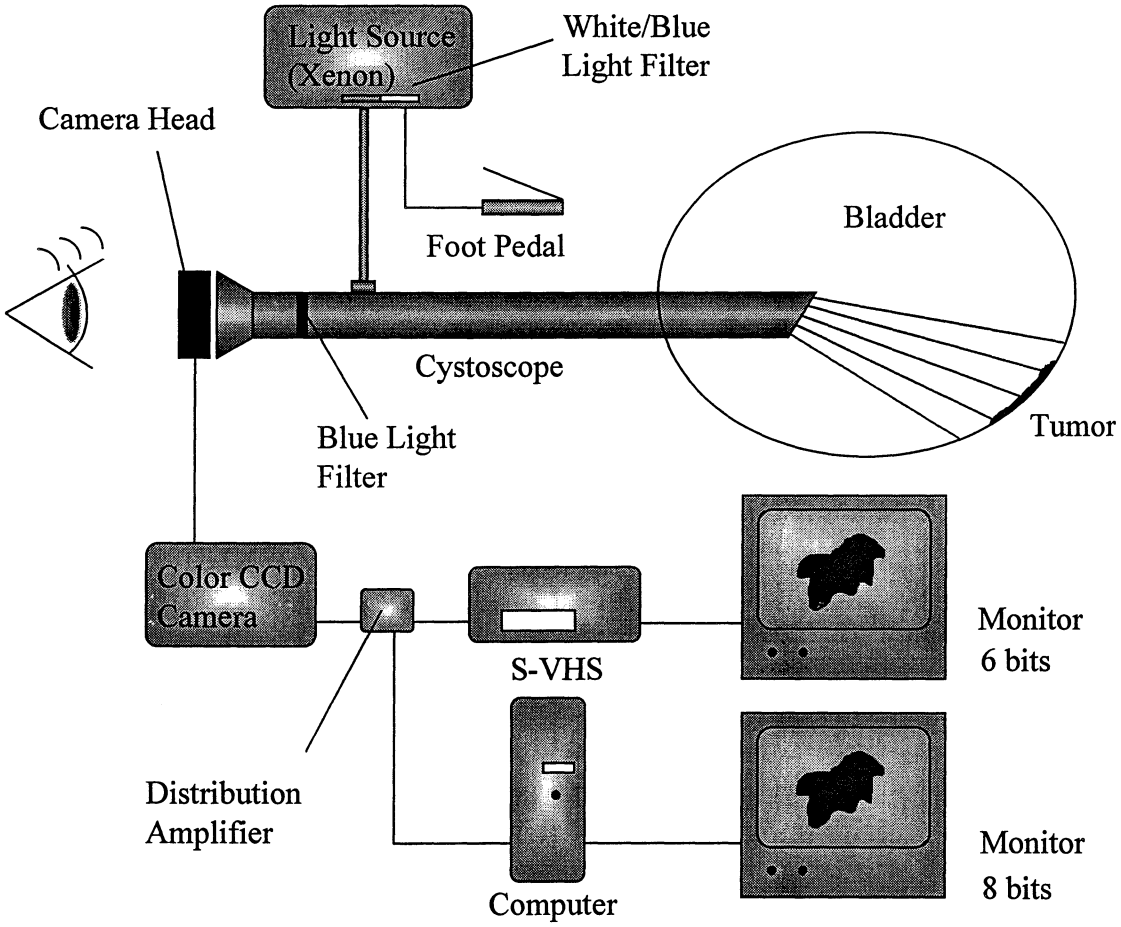

Figure 3.3. Equipment for measuring the ALA-induced PpIX fluorescence. A xenon-lamp with filters to switch between white and blue light with a foot pedal, is connected to the cystoscope. The red fluorescence light is detected through the eye piece, either with the naked eye, or with a CCD camera. Using a frame grabber, pictures were grabbed and processed.

Figure 3.3 shows a schematic illustration of the measuring equipment for the PpIX fluorescence. A light source (STORZ GmbH "D-light") containing a xenon-lamp, was used for excitation. By using a foot pedal it was possible to switch between two filters, giving white or blue light. This made it easy for the urologist to use white or blue light for illumination of the bladder and excitation of PpIX, respectively. Figure 3.4 shows the white and blue light spectra of the light source. The blue-light filter in the light source cuts out most light above 450 nm. This is desirable since the absorption peak of PpIX is around 400 nm, and the light above 450 nm only makes it harder to detect the much weaker red fluorescence from PpIX.

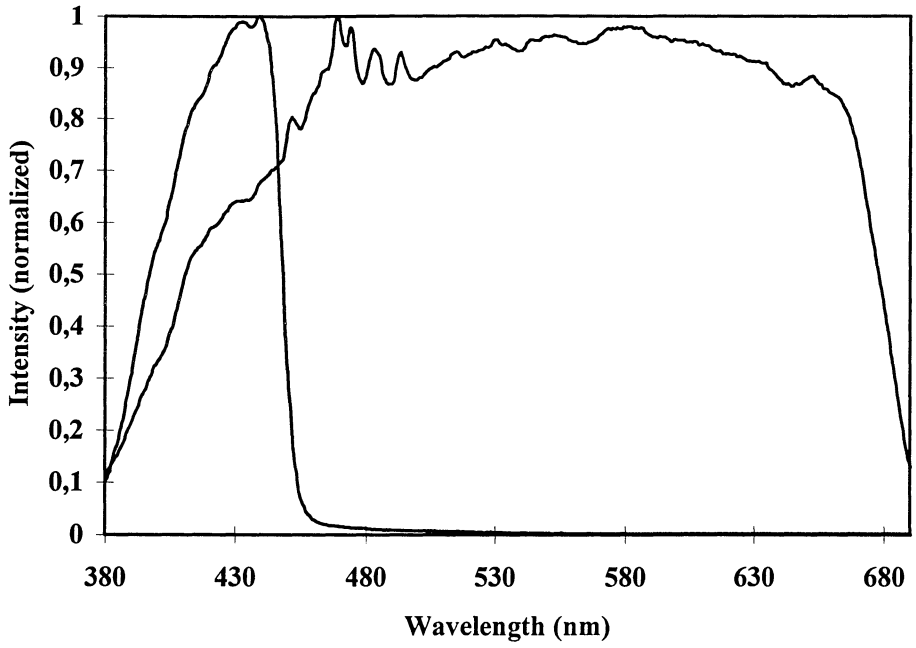

Figure 3.4. White and blue light spectra from the light source, STORZ GmbH "D-light". Both spectra are normalized, and thus, the intensities can not be compared. The blue-light filter in the light source cuts out most of the red light to make it possible to detect the weak red fluorescence from PpIX.

The optics of the cystoscopes (STORZ GmbH) had a built-in filter to discriminate against the blue excitation light. The filter cut out most of the blue light, allowing detection of the weaker red fluorescence. Three different cystoscopes were used in order to examine the entire bladder, one where the light left the scope straight ahead, 0°, one at a 30° angle and one at a 70° angle, see figure 3.5. The light guide was made of glass.

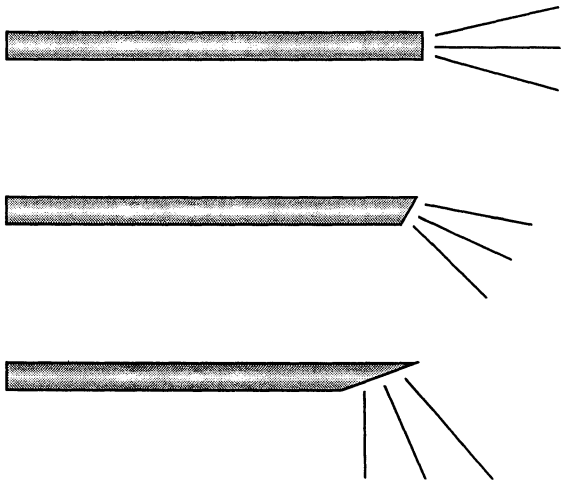

Figure 3.5. Three different cystoscopes were used for imaging the bladder, one where the light left the cystoscope at 0°, one at a 30° angle and one at a 70° angle.

3.3.4 Imaging System

The cystoscopes could be used for either visual observations by eye, or with a CCD camera attached to the eyepiece. According to the urologists, best results were obtained when looking by eye. When the CCD camera was used, there were sometimes problems with blurry pictures following long integration times. These long integration times were sometimes needed to get enough light on the CCD array. Obviously, these problems were avoided when looking by eye. Also, problems with saturation in the blue channel were eliminated when looking by eye.

Using a CCD camera, an Optronics CCD video camera system (P99300) connected to a computer, made it possible to grab pictures with a frame grabber, transfer the pictures to a computer and process them. The frame grabber used was a Matrox Meteor™ board together with Matrox Inspector™ software, which made it possible to grab color images, separate the red, green and blue components of the images and process these components separately. Pictures grabbed this way contained 8 bits of information in each color component. If the pictures were grabbed from the recorded tape (S-VHS VCR) instead, two bits were lost and only 6 bits of information per color component in each picture were obtained.

3.3.5 Procedure

To evaluate the method, two urologists were in the operating room. One urologist examined the bladder using both white and blue light, to see which areas were fluorescent. Then the other urologist, who did not see the result of this examination, did his ordinary cystoscopy, only using white light. By doing it this way it was possible to compare the ordinary white light procedure with the fluorescence method. Biopsies or resections were made on visible tumors, suspected areas and randomly chosen areas. When finished, the bladder was examined again with blue light to detect possible missed malignant or dysplastic areas.

3.3.6 Statistics

The sensitivity, specificity and positive and negative predictive values of white light cystoscopy, blue light cystoscopy and combined white and blue light cystoscopy for detection of malignant, including dysplastic, versus non-malignant urothelium, were determined with standard statistical methods.[28] See also appendix 4.

For statistical calculations with white light cystoscopy, areas that appeared hypervascular, papillary, raised or nodular were considered as positive macroscopic findings. Normal areas and scars were considered as negative macroscopic findings. Positive macroscopic findings during blue light cystoscopy were fluorescent areas.

When both white and blue light were evaluated, papillary and nodular areas that were found under white light, and hypervascular, raised and normal areas that were fluorescent under blue light, were considered as positive macroscopic findings. As

negative macroscopic findings hypervascular, raised and normal areas that showed no fluorescence and scars were chosen.

3.4 Results

Fifteen biopsies from frank papillary or nodular tumors and 32 biopsies from suspicious areas (average 2.9 biopsies per patient) were taken for pathological examination. Conventional pathological classification yielded 13 chronic inflammatory, 9 normal, 4 dysplastic (2 stage D2 and 2 stage D3), 2 hyperplastic and 19 malignant areas.

During blue light cystoscopy 20 of 23 true positive and 17 of 24 true negative areas were correctly identified. The 7 false positive areas were 1 hyperplastic, 2 normal, and 4 chronic cystitis (cC). The 3 false negative areas were all TaG2, see table 3.1. For terminology see appendix 2. The sensitivity of the method was 87% and the specificity was 71%. The positive and negative predictive values were 74% and 85% respectively.

One malignant and one dysplastic area missed during routine white light cystoscopy, but found during blue light cystoscopy, were macroscopically detectable and looked papillary and hypervascular. The third missed area (TaG1) was *not* possible to detect under white light. Of the 22 visually suspicious appearing sites 13 were fluorescent. Four of these were pathologically classified as non-malignant while 9 of the fluorescent sites were malignant or dysplastic (4 dysplastic, 5 Ta-1).

For white light cystoscopy the sensitivity was 87%, the specificity 38% and the positive and negative predictive values were 57% and 75% respectively. The missed areas during white light cystoscopy were 1 D2 and 2 TaG1.

White light cystoscopy		Fluor. cysto.	Pathology						
			Non-malignant			Malignant or dysplastic			
Macro.	WL pos	Fluor.	Normal	cC	hyp.pl.	D2	D3	Ta-1	T2+
Norm.	No	No	5	-	-	-	-	-	-
Norm.	No	Yes	-	1	1	-	-	1	-
Scar	Yes	No	-	2	-	-	-	-	-
Susp.	Yes	No	1	7	1	-	-	-	-
Susp.	Yes	Yes	2	2	-	2	2	5	-
Pap/nod	Yes	No	1	-	-	-	-	3	-
Pap/nod	Yes	Yes	-	1	-	-	-	8	2

Table 3.1. Number of bladder biopsies comparing macroscopic findings under white light cystoscopy in conjunction with fluorescence findings and pathological results. The column *"White light cystoscopy"* is divided into two columns; *"Macro." (macroscopic)*, which tells what the area looked like to the urologist, and *"WL pos." (white light positive)*, which indicates if the site was *possible* to detect under white light once it was found after blue light excitation. The column *"Fluor. cysto" (fluorescence cystoscopy)* indicates if the site was fluorescent when excited with blue light. The pathology classifications are divided into *"Normal", "cC", "hyp.pl.", "D2", "D3", "Ta-1"* and *"T2+"* which stands for *"Normal", "chronic cystitis", "hyperplastic", "dysplastic lesion, grade 2", "dysplastic lesion, grade 3", "papillary tumor, stage a or 1"* and *"papillary tumor, stage 2 or higher"*, respectively. The group *"Susp." (suspicious)* under macroscopic findings, include areas that looked hypervascular, raised and erythematous. The group *"Pap/nod"* include papillary and nodular tumors.

When both white and blue light were used for cystoscopy, the sensitivity was 100%, the specificity 67% and the positive and negative predictive values 74% and 100%, respectively.

A comparison between the three different procedures is shown in table 3.2.

	White light only	Blue light only	White and blue light
Sensitivity (%)	87	87	100
Specificity (%)	38	71	67
Pos. pred. value (%)	57	74	74
Neg. pred. value (%)	75	85	100

Table 3.2. Comparison of the sensitivity, the specificity and the positive and negative predictive values for cystoscopy using only white light, only blue light and both white and blue light.

Corresponding white and blue light pictures, showing one nodular tumor, one tumor which was hidden under an air bubble and one papillary tumor which did not show any red fluorescence, are shown in figure 3.6-3.8.

The visible malignant area which was hidden under the air bubble was missed during white light cystoscopy. Though, this tumor was strongly fluorescent under blue light and could be removed.

In figure 3.9 a line profile of the fluorescing flat lesion in figure 3.6 is shown. The software made it possible to make a straight line in the grabbed picture, and along this line, separate the red, green and blue components. The ratio of the red and green components (red/green) is roughly one or less in the regions surrounding the fluorescent area. In the fluorescent area though, the ratio is about two. The blue component is saturated. The signal-to-noise ratios of the red and green components are approximately 9.

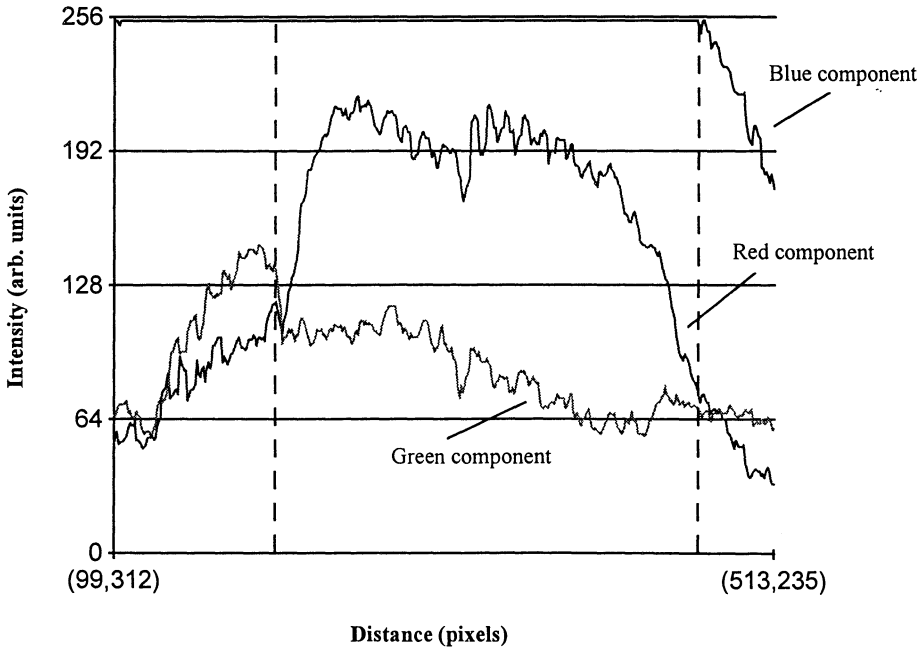

Figure 3.9. The red, green and blue components of the flat fluorescing lesion in figure 3.6. The dotted lines mark the malignant area. Note that the blue component is saturated. The signal-to-noise ratios of the red and green components are approximately 9.

In figure 3.10 the line profile from the papillary tumor in figure 3.8 is presented. This tumor did not show any fluorescence, which is seen in the red component which hardly increases at all in the malignant area. The blue component though, is much stronger in the malignant area than in the surroundings. The signal-to-noise ratios for the components are approximately 15. Calculations of the ratio of blue and green (blue/green) showed a clear difference between malignant and non-malignant areas, 0 in the surrounding areas, compared to more than 2 in the malignant area.

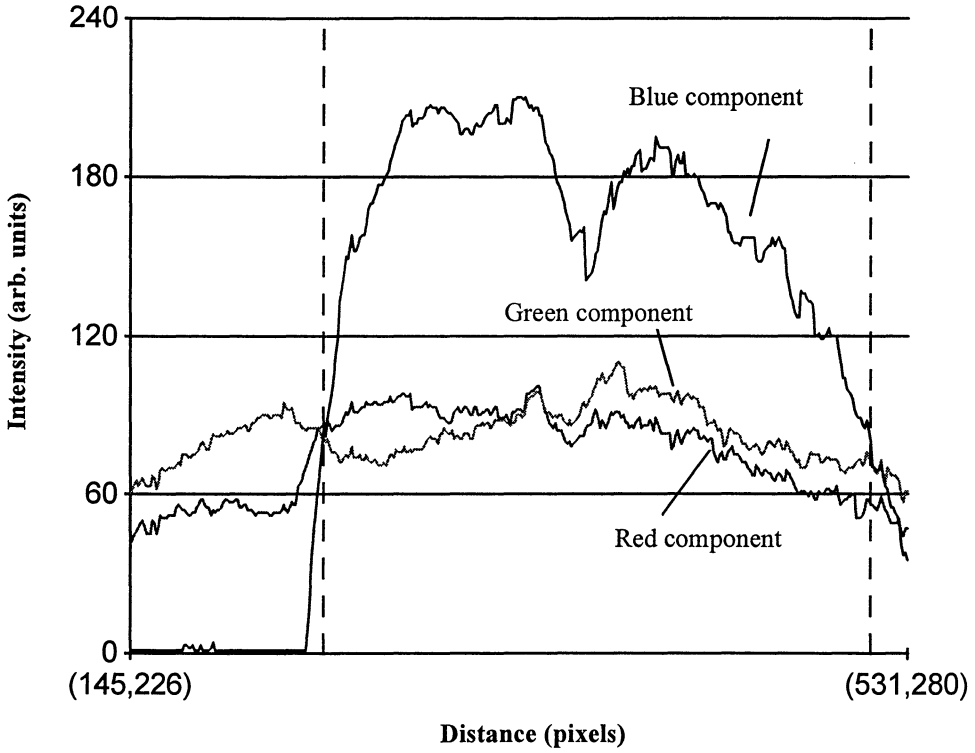

Figure 3.10. The red, green and blue components from the not fluorescent papillary tumor in figure 3.8. The dotted lines mark the malignant area.

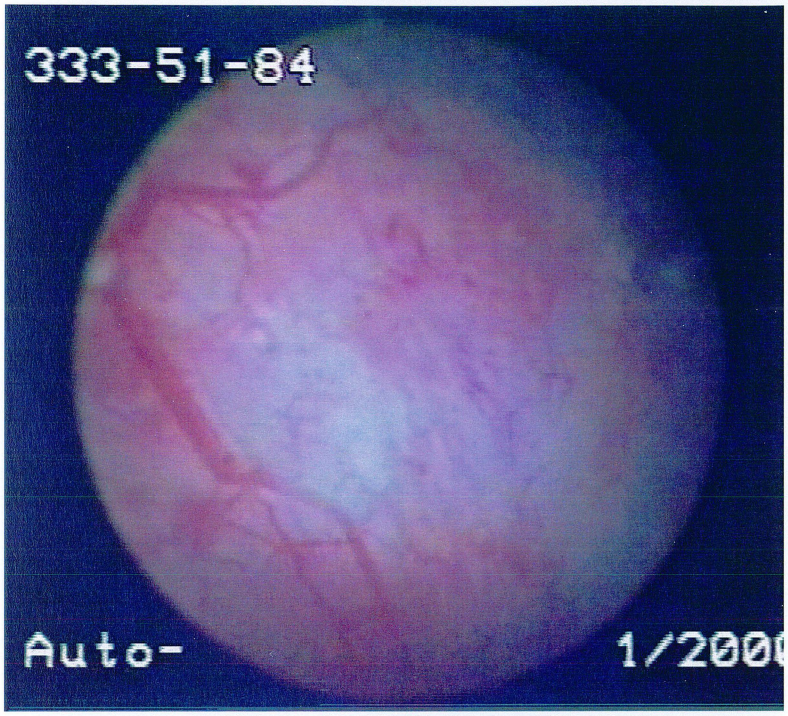

Figure 2.6 a. The figure shows a cancer tumor (TaG2) under white light. The tumor is barely visible and without distinct margins.

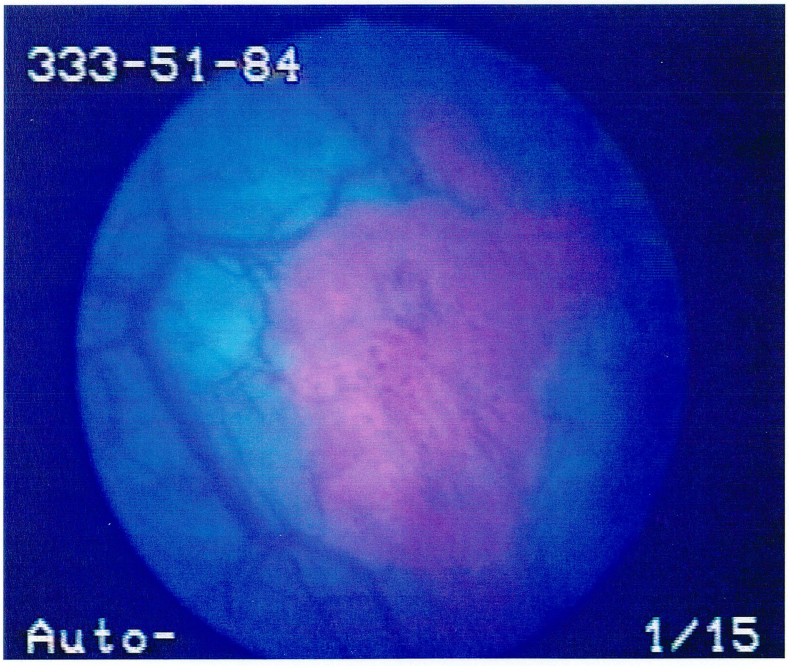

Figure 2.6 b. Under blue light the red fluorescence showed a wider area with sharp margins allowing a complete tumor resection.

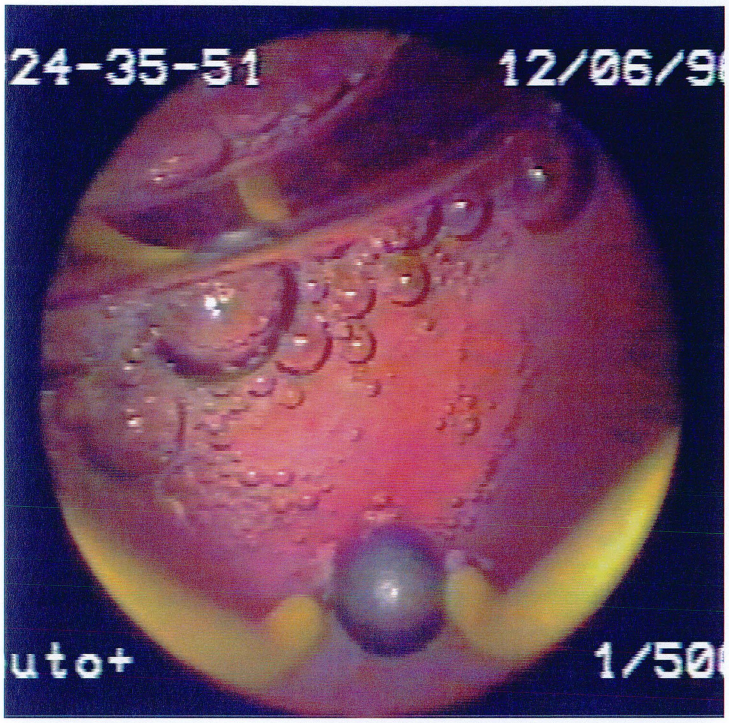

Figure 2.6 a. A cancer tumor under white light. The tumor was hidden under an air bubble and was missed during white light cystoscopy.

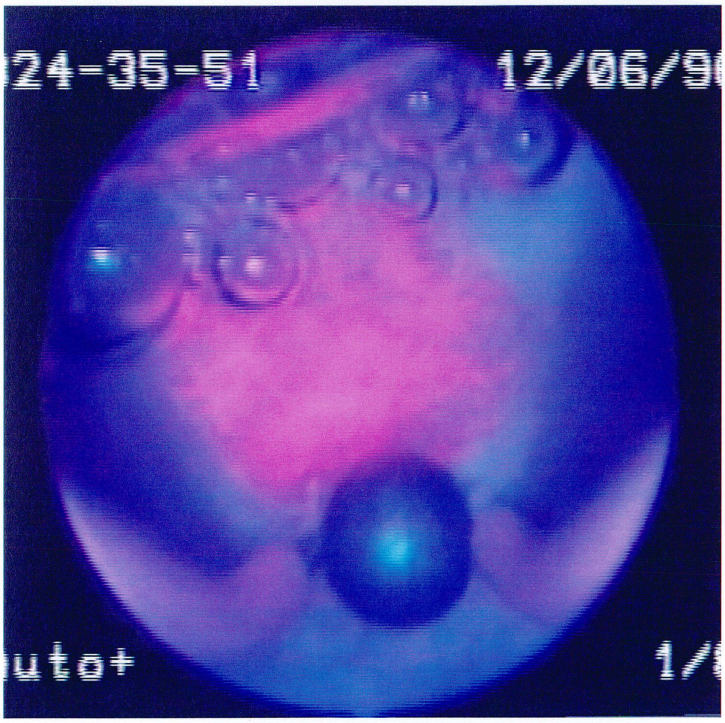

Figure 2.6 b. Using blue excitation light the red fluorescence revealed the tumor which was removed. The roller-ball in the picture is heated with a current and used for burning the tissue when the area is big. The diameter of the ball is approximately 5 mm.

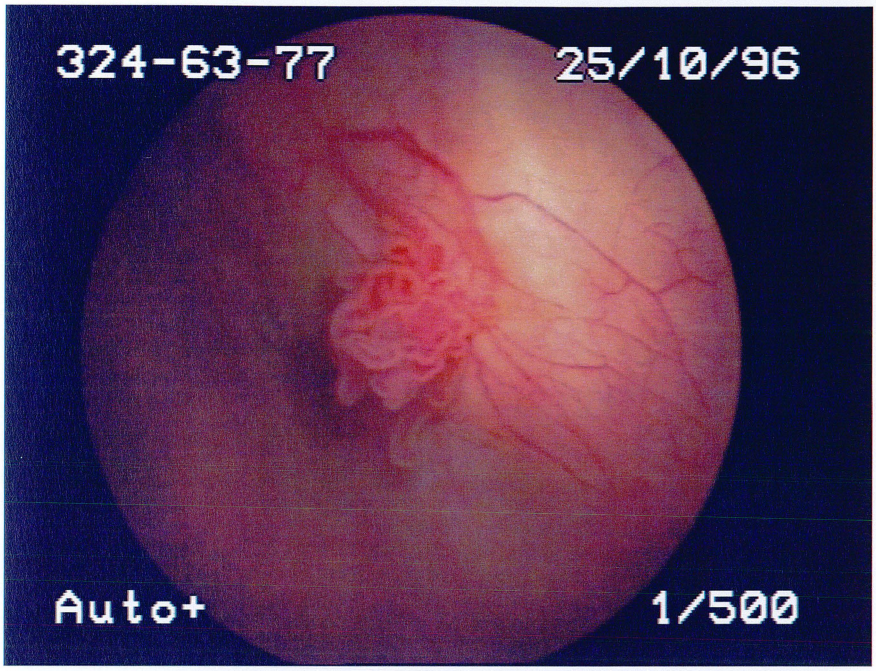

Figure 2.8 a. A papillary tumor under white light. The diameter is about 5 mm.

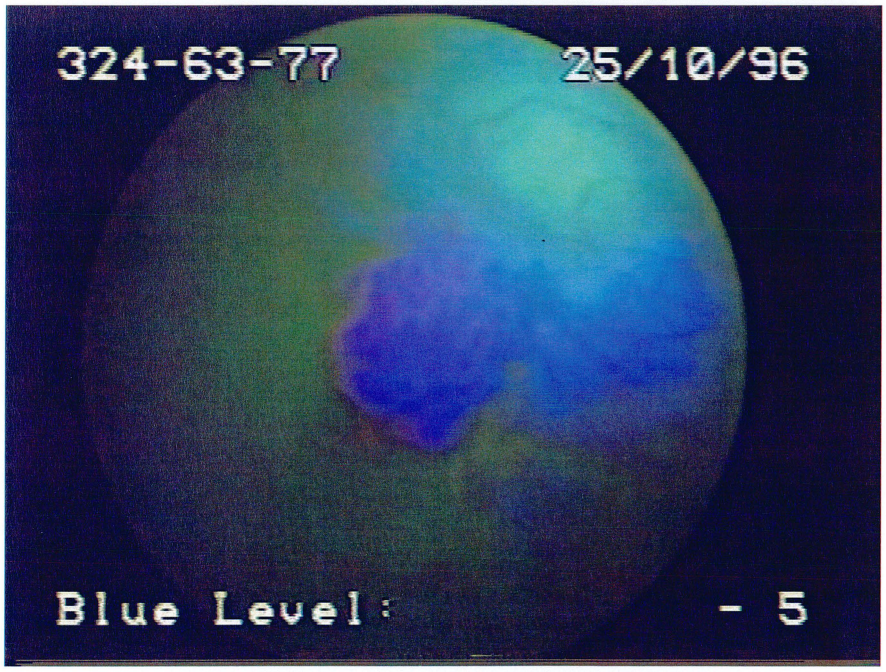

Figure 2.8 b. This papillary tumor showed no fluorescence during blue light cystoscopy. To increase the contrast between blue and red, the blue level was decreased, but still no red fluorescence was detected.

3.5 Discussion

Dysplasia, carcinoma *in situ* as well as small papillary tumors may be concealed in normal-appearing mucosa or by non-specific lesions in bladder tumor patients.[29] In that case ALA-induced PpIX fluorescence would be a helpful tool in detecting the malignant areas. Particularly, high grade dysplasias and carcinoma *in situ* have a crucial effect on the rates of progression and recurrence.[30-31] Whether it is important to detect dysplastic regions or not is debatable. They are not malignant areas, but considered pre-malignant, and may evolve to cancer in time.[32] In this investigation the dysplastic regions were included in the group the method was designed to detect.

Compared to other methods of fluorescence detection, fluorescence diagnosis with ALA has the advantage that the fluorescence can be discerned with the naked eye, so that elaborate image processing techniques are unnecessary. The easiness with which the PpIX is excited and the fluorescence detected, makes this method very easy to use. At the same time it gives the physician more confidence in removing all malignant and dysplastic tissue, and provide a great aid in detecting hardly visible or invisible lesions.

An ideal photosensitizer has no fluorescence to give maximum triplet yield, but most photosensitizers have fluorescence as well as triplet yield. Thus, most photosensitizers can be used for photodetection as well as phototherapy. The fact that both occur simultaneously can be a problem, since there might be a small risk that normal tissue could be destroyed as a result of the diagnostic procedure.

The technical requirements for this method merely comprise a blue light source in the region of the maximum fluorescence excitation spectrum of PpIX. Here a xenon arc-lamp with a corresponding filter was used. The decisive advantage of this light source was that the blue excitation light was directly coupled into the optical system of the endoscopes. Therefore, all conventional available endoscopic instruments could be used in combination with fluorescence diagnosis. This allows orientation and resection under violet excitation light, which, due to the high contrast, can be helpful since the entire extent of the tumor can not always be appraised with certainty under white light, see figure 3.6.

Under white light cystoscopy 15 of the 47 biopsies (32%) were non-malignant. During the blue light procedure only 7 (15%) were non-malignant. Using ALA-induced PpIX fluorescence, the number of biopsies from non-malignant sites, and hence also the invasiveness, could be decreased. The high sensitivity and negative predictive value for cystoscopy using both white and blue light might be due to the few random biopsies, only four.

In comparison to the results from Kriegmair *et al.* this study showed a higher sensitivity, 100% compared to 97% and the same specificity, 67%, see table 3.3.[19] Three false negatives (no fluorescence) were detected in this investigation. They were all papillary tumors, TaG2, and appeared papillary to the urologist.

	Results	Kriegmair's results
Sensitivity (%)	100	97
Specificity (%)	67	67

Table 3.3. A comparison of the sensitivity and the specificity for the combined blue and white light procedure with Kriegmair's investigation.

The line profiles made in this study were very few and performed to investigate the possibilities with the software. It seemed like the red and blue components had a higher intensity and the green a lower, in the marked malignant areas. If a more thorough study were conducted and a software which allows pixel by pixel calculations were used, it might be possible to enhance the contrast in a very simple way. This could then be done in real time in the operating room.

A solution to the problem with the saturated blue component in some of the line profiles could be to add a filter in front of the CCD detector. Already, in the cystoscope, there is a filter that cuts out some of the blue light to make it easier to detect the weak red fluorescence. If this filter would be replaced, or a new filter added which cuts out more of the blue light, the problem might be solved.

No side effects that would contraindicate widespread clinical use of the method were detected.

3.6 Conclusions

Due to the high sensitivity of the combined white and blue light procedure (100%), fluorescence guided biopsies are recommended instead of random biopsies. Using the white and blue light method, all found malignant lesions were detected and removed. But also additional non-malignant lesions were removed due to the low specificity, which is the obvious weakness of this method. The main point is that additional malignant and dysplastic lesions that were missed using only white light, were found using blue light. Eleven percent of the malignant and dysplastic lesions found using both white and blue light would have been missed using only white light.

The easiness with which the PpIX is excited and the fluorescence detected, and the fact that the fluorescence can be detected by the naked eye, make this method very useful and easy to use. Due to the high tumor selectivity of ALA, ALA-induced PpIX fluorescence is a very helpful tool in determining the exact extent of a tumor.

4 Diffuse Reflectance

4.1 Introduction

The possibility of using diffuse reflectance spectroscopy (DRS) in the wavelength region 400-700 nm to distinguish between malignant and non-malignant tissue was investigated. The hypothesis was that the amount of blood differs with tissue types, and also that the structure of vessels as well as the number and pattern of vessels are different, and that the detection of these variations is possible by looking at the spectrum of the diffusely reflected light. The hypothesis was that malignant and dysplastic lesions have a different vascular pattern compared to non-malignant tissue, including inflammatory lesions. This implies that if white light is shone at the areas of interest and the diffuse reflectance is measured, an altered blood absorption spectrum from the malignant and dysplastic areas compared to the non-malignant areas will be detected.

The reflectance of the tissue depends on several different properties of the scattering media, such as which chromophores (i.e. absorbers) and scatterers are present and in what concentrations. The major chromophore in bladder tissue is hemoglobin and the main scatterers are collagen and erythrocytes.[1]

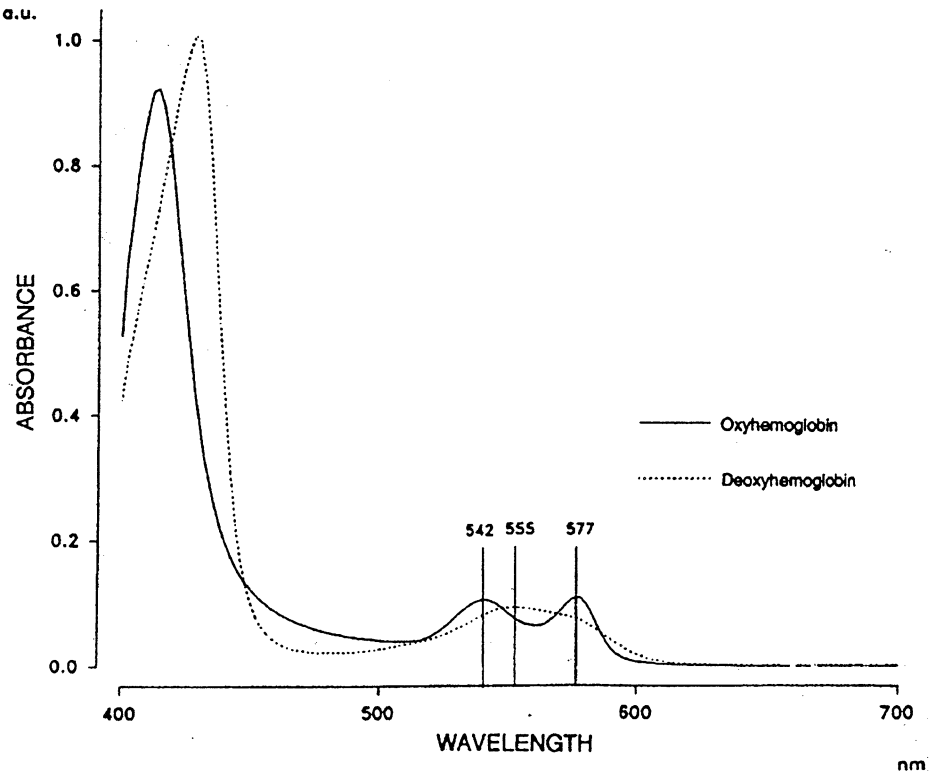

Figure 4.1. The absorption spectra of oxyhemoglobin and deoxyhemoglobin.[14]

The scattering in tissue is due to localized regions of different refractive index than the surroundings. Due to the relatively large size of the scatterers in the tissue, it is found that the scattering is highly forward directed.[2] On average the photon changes direction about 10° every time it is scattered, so before the back scattered light reaches the light collecting fiber every photon has experienced many scattering events.

The absorption in hemoglobin is very strong. In the visible and UV regions, deoxyhemoglobin (Hb) has an absorption peak at 555 nm and oxyhemoglobin (HbO_2) has two absorption peaks at 542 and 577 nm, respectively, see figure 4.1.

In the visible region, light penetrates several hundred microns into the urothelium and the underlying muscle layers. The penetration depth of the light was estimated to 1 mm based on earlier experiments made on the skin.[3] This means that the light penetrates through the urothelium, the basement membrane, the lamina propria and into the muscle, and is affected by the features of all these tissue layers, see figure 4.2.

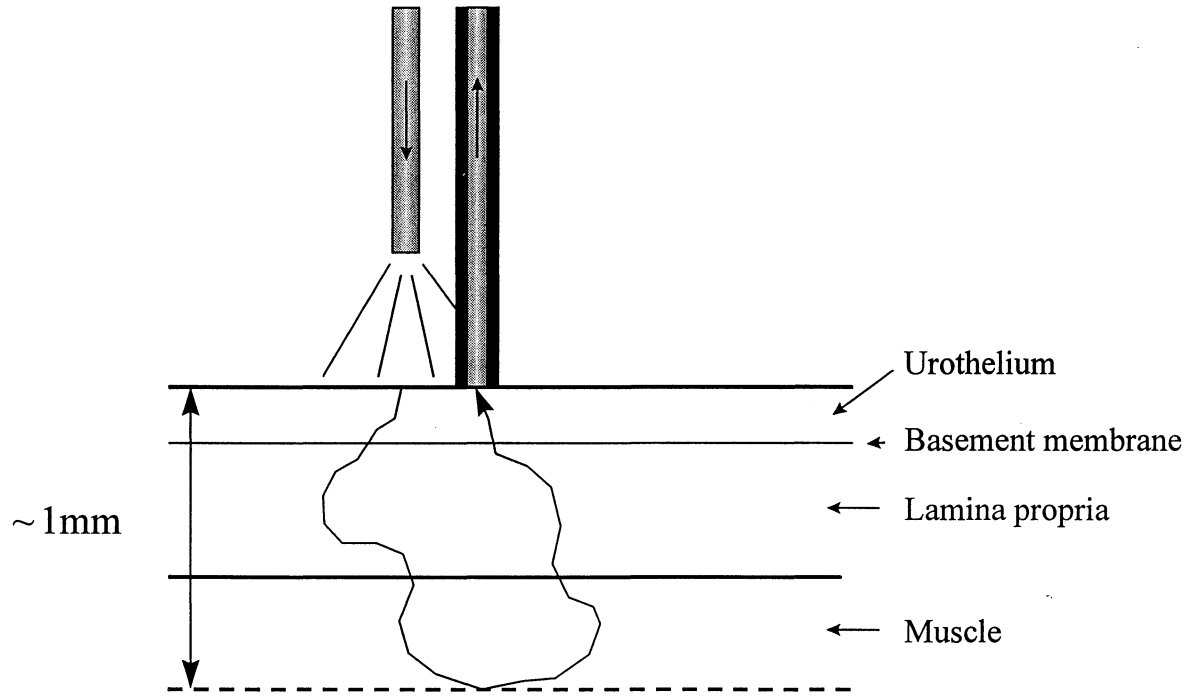

Figure 4.2. The detected light penetrates roughly 1 mm. This implies that with the geometry used, the average detected photon has penetrated the urothelium, the basement membrane, the lamina propria and entered the muscle.

For a unit irradiance the transmitted light T, into tissue is:

$$T = 1 - r$$

where r is the reflected light (Fresnel reflection). Some of the light that penetrates into the tissue will experience multiple scattering events and propagate in the backward direction and reach the tissue surface again. This light, which has not been absorbed by tissue chromophores, will be either internally reflected or transmitted at the tissue surface. The light that penetrates the surface again is called diffuse reflectance, see figure 4.3.

Thus, any measurement of reflection includes both the specular reflection above the irradiated tissue surface and the diffuse reflectance.

When light travels through tissue it may either be elastically scattered (no energy loss), inelastically scattered (energy loss) or absorbed. All three processes occur and their respective magnitudes depend on the scattering and absorption properties of the tissue, the wavelength of the light and on the intensity of the light. At intensities higher than used in these experiments stimulated scattering processes can occur. Examples of elastic scattering are Rayleigh and Mie scattering, while Raman scattering is an example of inelastic scattering. Tissues with different cellular structures are expected to have different elastic scattering spectra. Absorption features, which are a function of the biochemical properties of the tissue, are also readily seen in an elastic scattering spectrum if the photon path length is long enough.

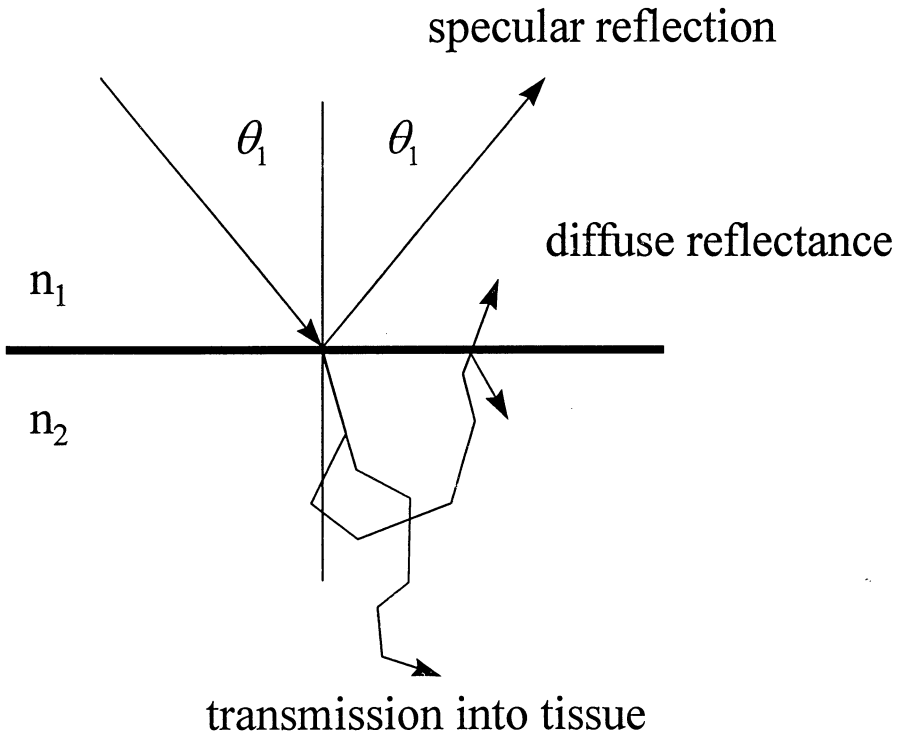

Figure 4.3. The incident light that is reflected in the surface is called specular reflection and the light that has entered the tissue, scattered many times and penetrated the tissue surface again is called diffuse reflectance.

By placing the light collecting fiber in gentle contact with the tissue, interference from specularly reflected light will be avoided and only light that has traveled through the tissue will be detected. This is desirable since specularly reflected light is not be negligible compared to the light transported through tissue and does not carry the spectral information of interest.[2]

Diffuse reflectance spectroscopy has been used in several *in vivo* experiments to assess potential clinical applications in various fields, ranging from measuring skin pigmentation to diagnosing diseases in the colon. Despite the relative simplicity and low

cost of the method, it can provide much information about the tissue examined. One must be very careful in the analysis of the data however, because of the complexity of the detected signals. Knowledge of the physical processes involved and the different tissue features such as the specific chromophores, the size and shape of the scatterers and the tissue structure are necessary to be able to correctly analyze the collected data.

The organ that has been subject to most experimental work is the skin. In contrast to other sites, skin contains not only hemoglobin but also the pigment melanin. The first reflectance spectrophotometry study of skin pigments *in vivo* was performed in 1939.[4]

Several quantitative measurements of skin color have been made since then.[5-7] The quantification of the pigmentation gives a measure of the concentration of melanin and the skin type could then be related to an index which would be a measure of the skin response to UV radiation, a topic studied extensively by dermatologists. This could replace the usual skin type number (I-IV), which is a more subjective measure of the concentration of melanin. This could then lead to a better understanding of which type of skin is likely to develop malignant melanoma and earlier preventive actions could be taken. However, the most effective way, by far, to reduce the risk of melanomas is to minimize the skin's exposure to solar UV radiation. Dermatologists have only limited success in diagnosing early malignant melanoma[8] and development of an objective diagnostic method could improve the success rate.

Diagnosis of pigmented lesions and melanomas with diffuse reflectance spectroscopy has been evaluated by at least five groups.[9-13] Because the scattering and absorption properties of the tissue depend on the biochemical composition and cellular and macroscopical structure, the malignant sites have been found to have different spectral features than healthy tissue.

Kollias *et al.* have used polarized photography and DRS methods to study inflammation in skin, specifically to evaluate the dose-response relation of irritant-induced erythema in skin.[13] The parameters used for the DRS were the changes in the apparent concentrations of Hb and HbO_2 in the skin and the results were compared with the photographs which were evaluated visually. The assumption was that the apparent absorbance is proportional to the chromophore concentration. Apparent absorbance $A(\lambda)$ is defined as

$$A(\lambda) = \log_{10} \frac{I_0(\lambda)}{I_{lesion}(\lambda)}$$

where $I_0(\lambda)$ is the reflected light from a reference and $I_{lesion}(\lambda)$ is the reflected light from the suspicious area.

This parameter was also used in another study in which Knoefel *et al.* studied the microcirculation of rat pancreas.[14] They used a fiber probe with the emitting and the receiving fibers randomly mixed. The recorded spectra were corrected for the scattering and the apparent concentrations for Hb and HbO_2 were then calculated. The configuration with randomly mixed fibers is expected to more evenly record the longer and shorter wavelengths than a probe with a thick emitting fiber in the middle surrounded by smaller collecting fibers.[14]

Coupling of the light into fiber optics enables use of reflectance measurements in endoscopic and laparoscopic procedures to study the walls of inner organs such as the gastrointestinal (GI) tract and the bladder. Several GI diseases are correlated with a

predisposition for cancer. Currently tissue biopsies are necessary in order to make the diagnosis. These biopsies, sometimes randomly taken, are time consuming and involve a risk for the patient. Optical diagnostic techniques for "guided biopsies" could be more specific for malignant lesions than random biopsies.

Mourant *et al.* have used a double fiber probe in their optical biopsy system. The system has been used to study human bladder *in vivo*.[15] The white light from a pulsed xenon point-arc lamp is coupled into one of the fibers. The probe is placed in contact with the tissue and the diffuse backscattered light is collected by another fiber adjacent to the first. The size of the probe is roughly 2 mm which allows it to pass through a working channel of a cystoscope. The group has conducted a study of human bladder cancer *in vivo* with a reported sensitivity of 100% and specificity of 97% for differentiation between malignant and non-malignant tissue. Their study included 10 patients (20 malignant and 30 non-malignant sites). Their algorithm used the slope of the spectrum of the backscattered signal in the wavelength region of 330-370 nm for correlation with pathology. They have also studied several locations in the GI tract, such as the colon/rectum, the esophagus and the stomach.[16] For the colon/rectum the reported sensitivity was 100% with a specificity of 96% for the 6 malignant and dysplastic lesions examined in the 16 patients included in the study. Other potential applications of their system have also been studied by the group, e.g. locating the transition zone between columnar and squamous cell epithelia near the opening of the cervix. Another application of reflectance is the monitoring of the oxygenation of blood (reflectance pulse oximeter).[17-18] This is for instance used during operations under an anaesthetic.

To be able to deduce any results, the penetration depth of the light used must be known. Otherwise it is not known what tissues are examined and it is not possible to correctly analyze the detected signals. The recorded signal is a sum of all the backscattered light from the so called sampling volume. This sampling volume is determined by the geometry of the measuring system and the wavelength of the light used.

Most of the reflectance experiments are using fiber probes of various geometry. Mourant *et al.* used a dual fiber system which is placed in contact with the tissue.[15] Knoefel *et al.* used a fiber bundle where the emitting and receiving fibers were randomly mixed[14] whereas Wallace used an organized arrangement of the fibers within the probe[9]. The different geometries could give different results because of the altered sampling volumes in the tissue and the different responses to different wavelengths. The varying volumes also give rise to different filtering in the tissue due to altered path lengths. Also the diameter and the numerical aperture of the fibers used affects the sampling depth.[19] A collection of thinner fibers sample more superficially than a thicker one. The results from different measuring geometries are very difficult to compare.

Common light sources are xenon-, tungsten-, tungsten/halogen- and deuterium-lamps, which have a high output in the visible region. To get an image of the examined area, a CCD camera combined with a filter arrangement could be used. This was proposed by Andersson *et al.* in 1987[20] and also used by e.g. Marchesini *et al.*[7]

4.2 Materials and Methods

4.2.1 Patients

Diffuse reflectance measurements were performed in 21 patients with bladder cancer undergoing mucosal biopsies or transurethral resection of the bladder at initial diagnosis or at regular bladder tumor follow up visits. Average patient age was 71 years (range 53 to 86 years).

4.2.2 Equipment

For the reflectance measurements a xenon-lamp based light source from Pilling, Luminator™, was used to illuminate the tissue, see figure 4.4. A standard cystoscope (STORZ GmbH), and the same OMA-system (modified) as described earlier in the autofluorescence chapter was used to measure the reflectance spectra.

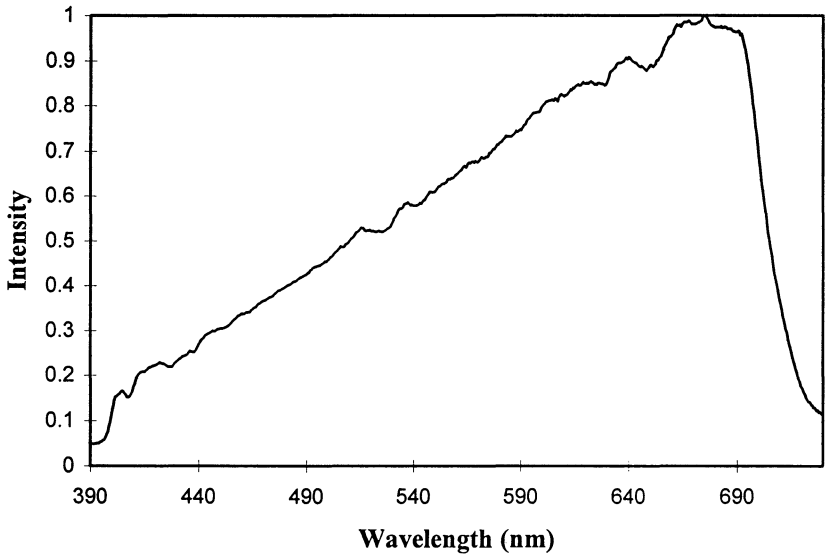

Figure 4.4. Normalized white-light spectrum from Pilling's Luminator™ light source, background subtracted and corrected for system response. The drop in intensity around 400 nm is due to absorption in glass fibers.

A compromise between ideal measuring conditions and what was possible in the operating room was made. The shortest possible exposure time, 16.634 ms/scan and an empirically determined distance between the scope tip and the tissue surface of 20 mm was used in order not to saturate the diode array. Because the reflected light was much stronger than the fluorescence light, an additional neutral density filter (ND 1.2) that blocked out 94% of the light* was required using this geometry. This filter was placed in

* The transmittance $T=10^{-1.2}=0.063$, which gave an attenuation factor of 94% (100%-6.3%≈ 94%).

front of the first lens in the setup, see figure 4.5. As many recording scans from each position as possible were preferable to increase the signal-to-noise level, but also the fact that the patients were under an anaesthetic had to be considered, and therefore the time could not be too long. A short measuring time was also important because the urologist was going to perform three procedures at the same spot, fluorescence and reflectance measurements and a biopsy. Fifty scans provided a sufficient signal-to-noise ratio, 40, yielding an integration time of less than one second.

In the bladder the cystoscope was used to shine light on the target and an optical fiber (0.6 mm quartz fiber) was used to collect the diffuse reflectance. To prevent cross talk, i.e. light from the cystoscope without any interaction with the tissue, entering the fiber through the fiber walls instead of through the fiber tip, an opaque catheter was placed around the fiber and fixed in position by glue, see figure 4.6. On the catheter there were black marks at every 10 mm and these marks were very useful in helping the surgeon keep the same distance between the fiber tip and the cystoscope at every measurement. By keeping the measuring geometry the same, equivalent light intensity at the tissue from measurement to measurement was ensured.

To measure the diffuse reflectance spectra the urologist put the light collecting fiber in gentle contact with the tissue and also reported what the site looked like. In every bladder the suspicious sites as well as some normal looking areas were measured. Usually, no biopsies were taken from the normal looking areas. The reflectance spectra obtained from lesions were referenced both to reflectance spectra from normal areas and to the light reflected from white gauze.

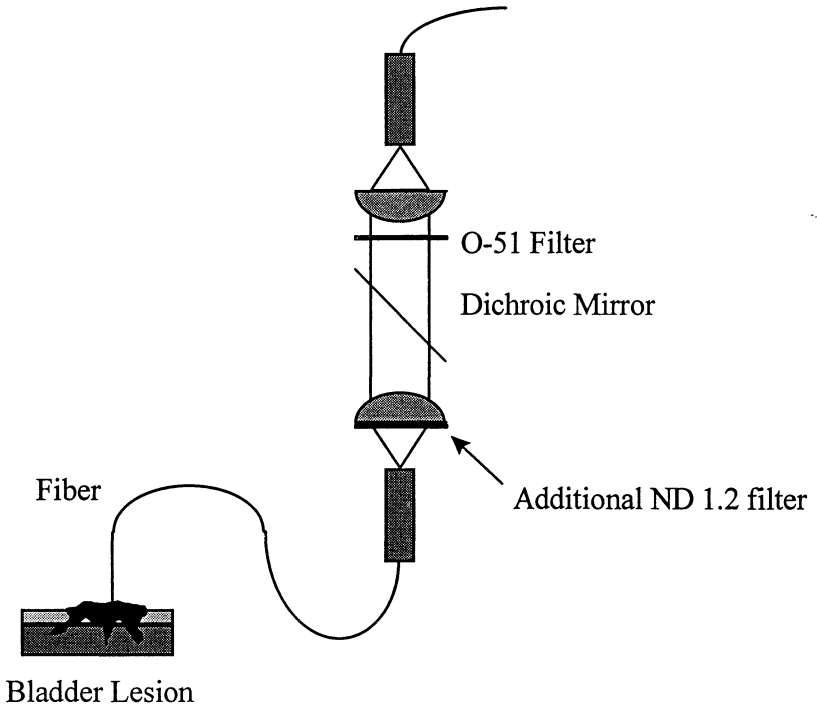

Figure 4.5. The additional ND 1.2 filter was placed in front of the first lens and blocked out 94% of the light so the detector would not be saturated.

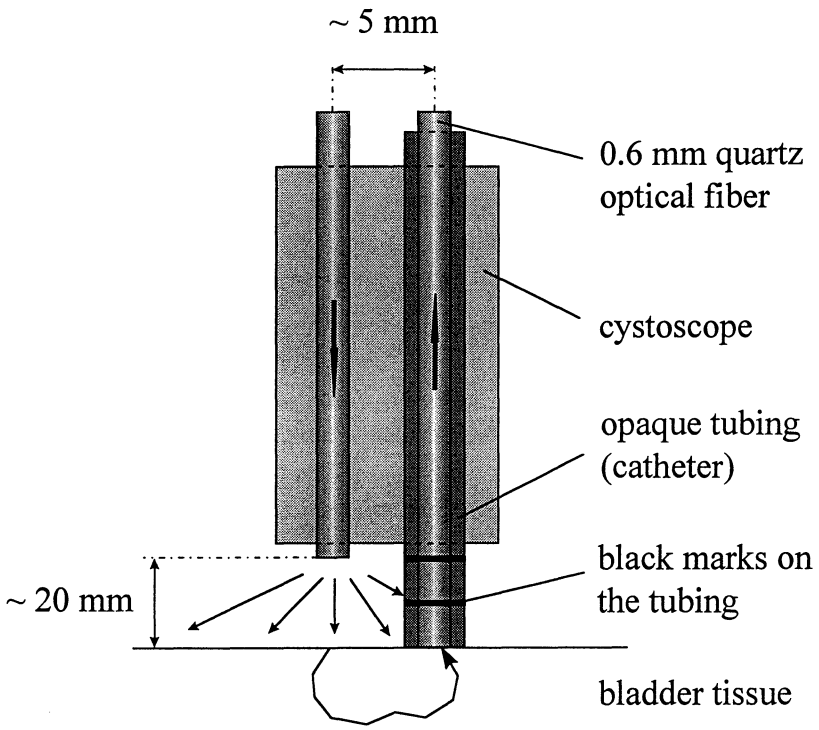

Figure 4.6. The arrangement of the cystoscope and the optical fiber. The distance between the tip of the light guide and the tissue surface was ~ 20 mm and the distance between the light guide and the light collecting fiber was ~ 5 mm.

4.2.3 Apparent Absorbance

To determine the concentration of light absorbers in the tissue, the apparent absorbance $A(\lambda)$, was calculated as

$$A(\lambda) = \log_{10}\left(\frac{I_{gauze}(\lambda) - I_{background}(\lambda)}{I(\lambda) - I_{background}(\lambda)}\right)$$

where λ is the wavelength, $I_{gauze}(\lambda)$ is the light reflected from white gauze, $I_{background}(\lambda)$ is the light intensity measured with the light source turned off, i.e. the light from the operating room leaking into the optics and $I(\lambda)$ is the measured signal from the area of interest, at the same wavelength. White gauze was used because of convenience and since it is known to be a good white light reflector with reproducible reflection characteristics. $A(\lambda)$ is referred to as the apparent absorbance because the diffusely reflected light intensity depends on both the absorbance of the specimen present as well as the scattering.[14] To exclude the influence of scattering, all obtained spectra were corrected for the wavelength-dependent scattering in the following way

$$A_c(\lambda) = A(\lambda) - (a + m \cdot \lambda)$$

where $A_c(\lambda)$ is the apparent absorbance corrected for the wavelength-dependent scattering, m is the slope of the least squares fitted line to the data between 640 and 680 nm and a is

the intercept of this regression, see figure 4.7. By correcting this way, the scattering is approximated with a linear wavelength-dependence, which between 500 and 700 nm is thought to give sufficiently accurate results.

The extinction coefficients of Hb and HbO_2 are 50 times smaller at wavelengths longer than 640 nm than in the range between 540 and 580 nm.[21] There are also no other chromophores in the tissue that have an appreciable extinction coefficient in this region, and hence, do not contribute much to the slope of the spectrum in this area. The apparent absorbance in the range between 640 and 680 nm is thus mostly due to scattering. This region was therefore chosen for background scattering correction in this study.[14] Towards longer wavelengths the intensity of light is distributed in a larger volume and less light reaches the light collecting fiber. This wavelength-dependent scattering coefficient is what gives the negative slope of the scatte correction line.

For the analysis of the concentrations of Hb and HbO_2, the extinction coefficients at 555 and 577 nm were used instead of the much higher values at 415 and 430 nm. The shorter wavelength range might have offered more reliable measurements but the penetration depth at 415 and 430 nm is much smaller than at 555 and 577 nm, yielding a more shallow probe volume. Light penetration at 555 and 577 nm is approximately 1 mm.[3] Also, the light source did not give enough light in this wavelength region.

After correcting for changes in scattering, differences in the spectra should be primarily due to changes in concentrations of Hb and HbO_2. The apparent absorbance can be described as a linear combination of Hb and HbO_2 as

$$xH_o(\lambda) + yH_d(\lambda) = A_c(\lambda)$$

where $H_o(\lambda)$ and $H_d(\lambda)$ are the absorbance reference spectra of pure HbO_2 and Hb, respectively. Reference wavelengths were the 577 nm maximum of the HbO_2 absorbance and the 555 nm maximum of the Hb absorbance.[21] The concentrations of HbO_2 (x) and Hb (y) were determined solving the following system of linear equations

$$xH_o(555) + yH_d(555) = A_c(555)$$
$$xH_o(577) + yH_d(577) = A_c(577)$$

and the O_2-saturation (the percentage of HbO_2 in the blood) was calculated as

$$O_2 - saturation = \frac{x}{x+y}.$$

For a given geometry of the scope and the fiber, the fraction of the illumination photons entering the fiber at each wavelength depends on the scattering cross section and anisotropy, as well as the absorption coefficients of the tissue components. The scattering anisotropy is the angular dependence of the scattering. There might be a greater probability for scattering in some directions than others.

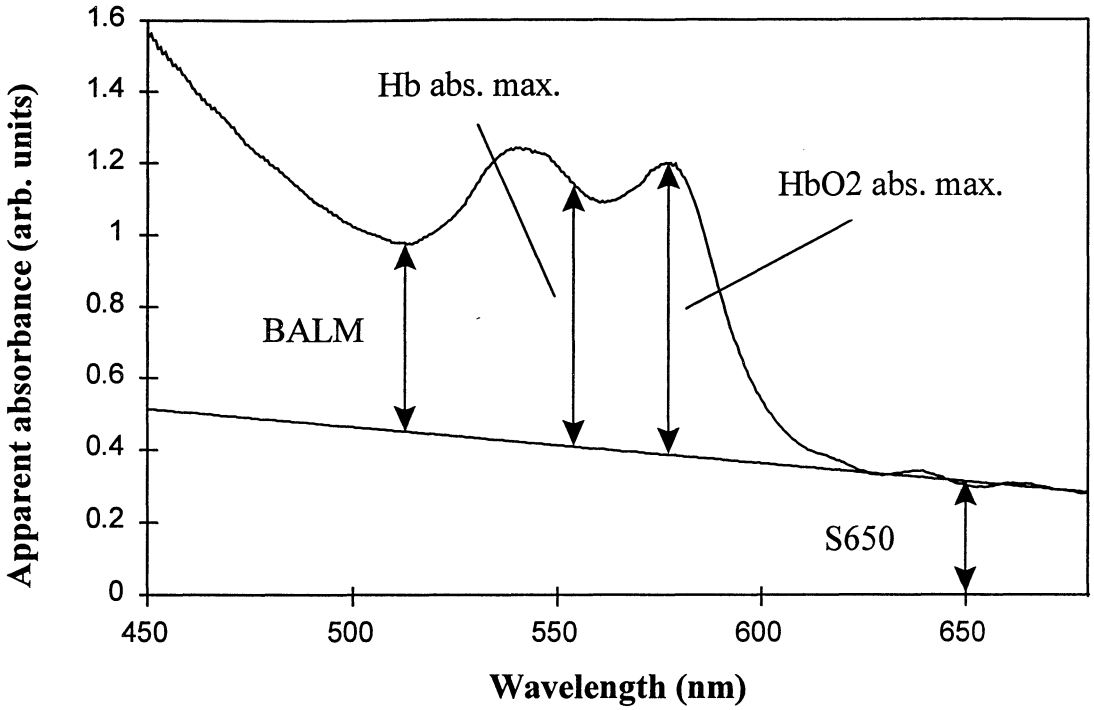

Figure 4.7. Figure showing how the blood absorption at the local minimum around 515 nm (BALM), the scattering at 650 nm (S650) and the Hb and HbO_2 absorption were measured. The fitted line for scatter-correction is also displayed in the figure.

For every measured site the concentrations of Hb and HbO_2, respectively, the total concentration of blood, the O_2-saturation and the slope of the fitted line were calculated. Also, the intensity of $A_c(\lambda)$ at the local minimum around 515 nm and the intensity at 650 nm, were determined. They were labeled BALM (blood absorption at local minimum) and S650 (scattering at 650 nm), respectively, see figure 4.7. The slope of the fitted line is an estimation of the wavelength dependence of the scattering, i.e. the size of the scatters, while the S650 is an estimation of the concentration of scatters.

4.2.4 Relative Absorbance

The reflectance from suspicious areas was also compared to normal areas from the same bladder. By doing so the variations from patient to patient, and also the small error introduced by assuming the reflectance of gauze to be 100% for all wavelengths, were removed. The relative absorbance $A(\lambda)_{relative}$, was calculated as

$$A(\lambda)_{relative} = \log_{10}\left(\frac{I(\lambda)_{normal} - I(\lambda)_{background}}{I(\lambda)_{lesion} - I(\lambda)_{background}}\right)$$

where $I(\lambda)_{lesion}$ is the spectrum from the suspicious area, $I(\lambda)_{normal}$ the spectrum from the normal area and $I(\lambda)_{background}$ is the background spectrum measured with the light source

turned off. A signal was still measured although the light source was turned off. This was due to leakage of light from the operating room into the OMA optics.

The deviation of the relative absorbance at 577 nm (HbO_2 absorption maximum) from the line fitted to the flat region between 620 and 700 nm and the offset (the deviation from zero at 650 nm, of the fitted line) were calculated to tell if there were any consistency between different lesions, see figure 4.8.

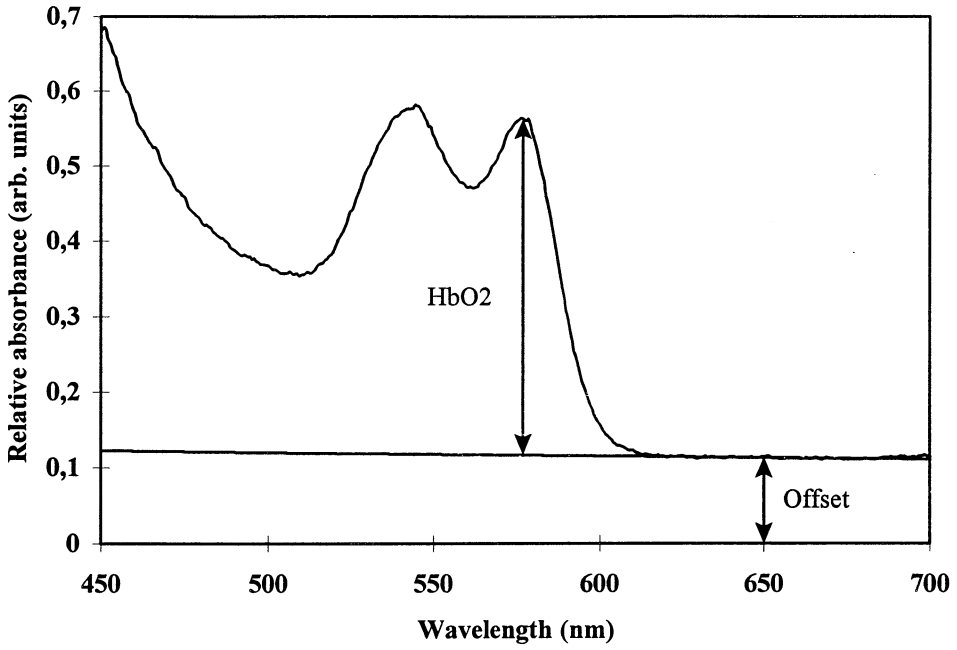

Figure 4.8. Figure showing how the relative absorbance of HbO_2 and the offset were measured.

4.2.5 Statistics

The sensitivity, specificity and positive and negative predictive values of diffuse reflectance measurements for detection of malignant, including dysplastic, versus non-malignant urothelium were determined with standard statistical methods. To obtain the significance of reflectance differences between groups of different tissue types, a standard Student t-test (2-tailed, equal variance) was used, and the significance was defined at $p<0.005$.[22]

4.3 Results

Fourteen patients were eligible for the study, with a total of 26 sites (1.9 sites per patient). Five of the included normal sites were not confirmed by the pathologist because no biopsies were taken. As determined by pathological classification of the eligible sites, there were 7 chronic inflammatory, 1 normal, 2 squamous metaplastic, 2 dysplastic (stage D2), 5 malignant (2 TaG2, 1 T1G3 and 2 T2G3) areas and 4 carcinoma *in situ*.

In figure 4.9 the raw data (corrected for background and system response) from a diffuse reflectance measurement of one T1G3 tumor and one normal site in a bladder is presented.

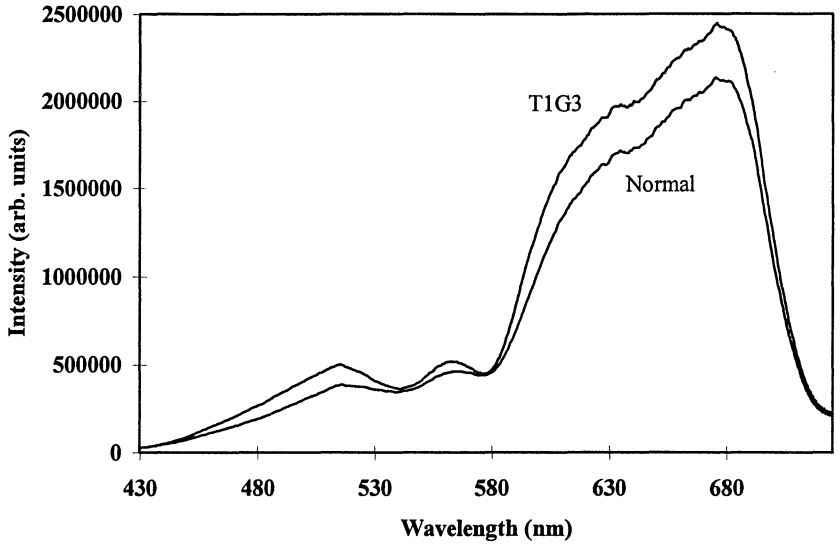

Figure 4.9. Diffuse reflectance measurements from one T1G3 tumor and from one normal area in a bladder. The spectra are background subtracted and corrected for system response.

Figure 4.10 shows the calculated apparent absorbance spectra from one Cis, one malignant tumor (T1G3) and one normal area from the same human bladder. The least squares fitted lines for the scatter-corrections are also shown.

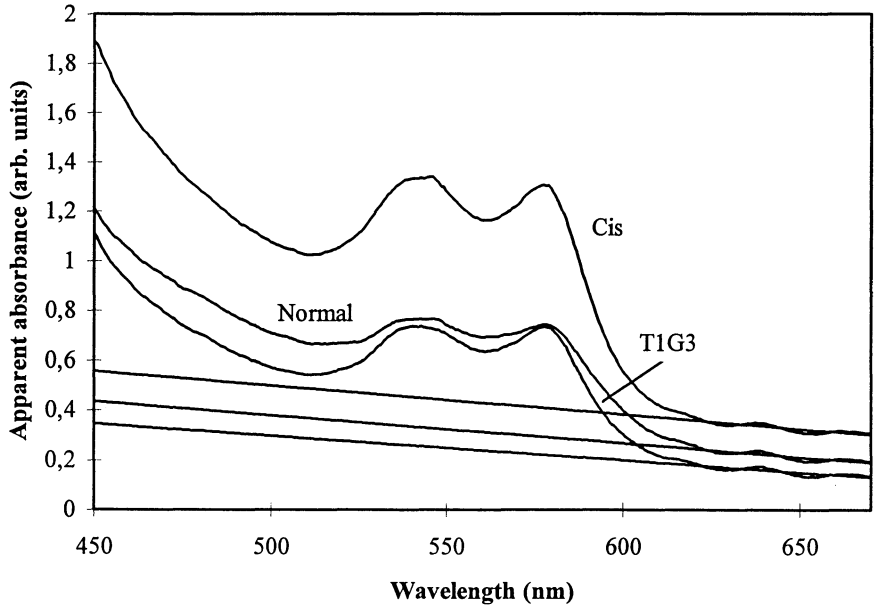

Figure 4.10. Calculated apparent absorbance spectra from one Cis, one T1G3 and one normal area. The scatter-correction lines are also displayed.

High apparent absorption was found around 540 and 569 nm corresponding to the α and β absorption bands of HbO_2.

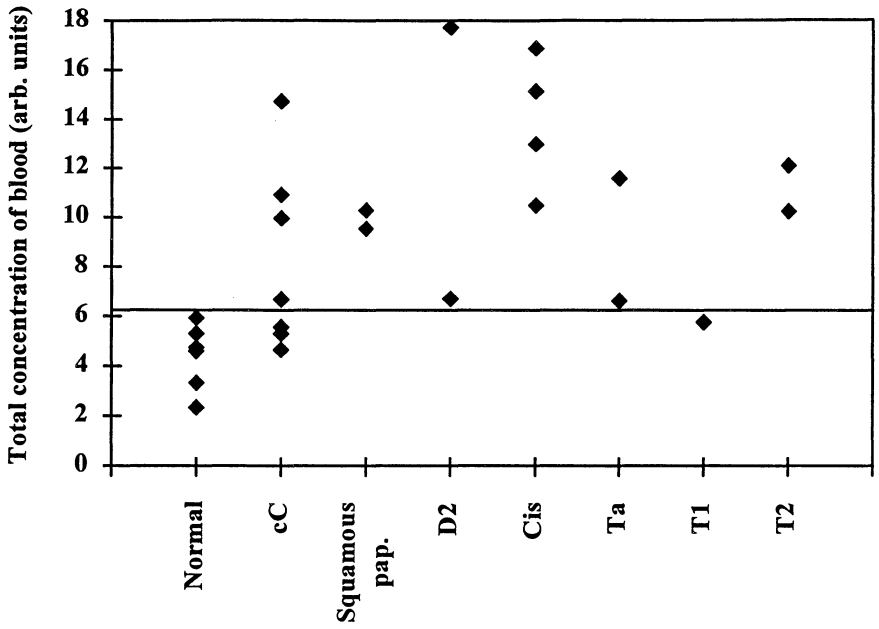

Figure 4.11. Scatter plot showing the total concentration of blood for the 26 measured areas (pathologically confirmed apart from some normal areas) from 16 patients.

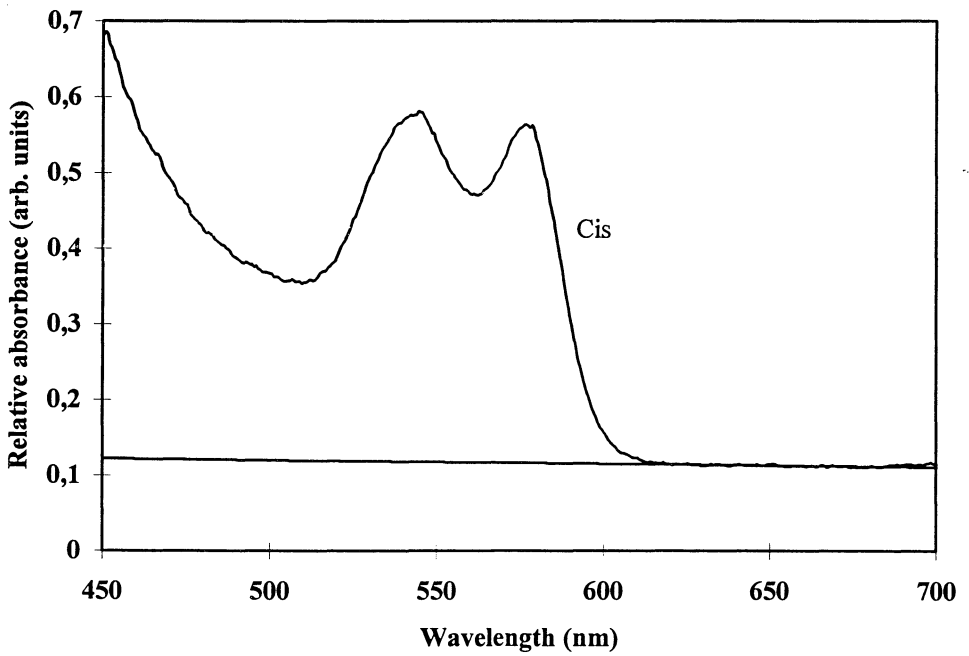

Figure 4.12. Relative absorbance from a Cis with the offset line fitted to the flat area between 620 and 700nm. Both the measurement from the Cis and the measurement from the normal area used in the calculation of the relative absorbance are background subtracted.

The results of the calculations of the BALM, the S650, the concentrations of HbO_2 (x) and Hb (y), the total concentration of blood (x+y), the O_2-saturation and the slope of the fitted scatter-correction line, indicated that only the total concentration of blood showed good separation between malignant and non-malignant areas. In figure 4.11 a scatter plot of the total concentration of blood for the 26 measured areas is shown.

The number 6.2 was empirically chosen to distinguish between malignant and non-malignant areas. This gave 10 true positive, 6 false positive, 9 true negative and 1 false negative area. Calculations showed a sensitivity of 91%, specificity of 60%, positive predicted value of 63% and a negative predicted value of 90%. However calculations of the concentration of blood did not show a clean difference between malignant and inflammatory areas. The mean values of the total amount of blood found for malignant, including dysplastic, and non-malignant tissue were significantly different ($p<0.005$). The calculations of the relative absorbance did not show any separation between malignant and non-malignant tissue. Neither the offset nor the HbO_2-absorption showed any consistency between different types of tissue. In figure 4.12 a typical calculated relative absorbance spectrum from a Cis is shown.

4.4 Discussion

This study was conducted to investigate the possibility of using DRS to diagnose bladder lesions. Most earlier studies have used a probe with a central light emitting fiber and peripheral receiving fibers. Instead of this arrangement Knoefel *et al.* used a probe of randomly mixed fibers[14] that more equally recorded shorter and longer wavelengths. In this study the possibility of using the cystoscope lamp as excitation source was investigated. By doing so, an additional light source would not be needed, but the same source as supplied with the cystoscope could be used.

The reason for using the same intensified diode array as for the autofluorescence measurements, although such a sensitive system was not needed, was that it was available. A CCD array would have been enough, and maybe even better since the problem with saturated signals maybe would have been avoided and the stronger signals would have given a better signal-to-noise ratio. It is also possible to connect a CCD array directly to a computer and to process the data on-line. The CCD array and the computer could be designed to be small with minimal cost. One disadvantage with the detection geometry used was that the light collecting fiber slightly shadowed the bladder tissue so the measured area was not evenly illuminated.

The light source used in this study emits light above 400 nm. By using a light source that emits further into the ultraviolet region, it might have been possible to investigate other wavelength regions. Of course, in that case the light absorption in the fibers must also be taken into account. Mourant *et al.* found that the most reliable spectral signature for detecting malignancy in the bladder using diffuse reflectance, was in the region 330-370 nm.[15] They found a sensitivity of 100% and a specificity of 97%, though their study included only 10 patients. A danger using these short wavelengths, down to 300 nm, is that malignancies could be induced.

Since biopsies are usually not taken from normal areas, only one of the so called normal areas was confirmed by a pathology report. The other normal areas were areas that visually gave a normal impression to the urologist.

Using a white light source, an increased concentration of highly absorbing blood would lead to a decreased detected signal. This is thought to be the case in inflammatory tissue. When the concentrations of Hb and HbO_2 were calculated, no discrimination between different types of lesion was found. Though, when the concentration of blood (both oxy- and deoxyhemoglobin) was calculated, a significant difference between normal and abnormal areas was shown. This is not surprising since the areas that are termed normal are those which do not look red and red areas appear red just because they contain more blood. Though, the measurements might provide more information than visual observations, since the fiber detects light that has penetrated deeper than the light detected by the human eye. The calculations of the O_2-saturation did not show any difference between different lesions.

The calculation of the slope of the apparent absorbance in the wavelength region between 640 and 680 nm, shows the wavelength dependence of the scattering. Since the sizes of the scatterers determine the wavelength dependence, these calculations give an estimate of the scatterers' sizes. The results, though, indicated no differences in sizes between the scatterers in different lesion. To determine the concentration of scatterers, the S650 was calculated. These calculations showed that the concentration of scatterers is about the same in various lesions. The local minimum in the apparent absorbance around 515 nm was also determined for the different measurements. Also here, no consistency between various lesions was found.

The results from the relative absorbance calculations did not show any consistent deviations between different lesions, neither the relative absorbance of HbO_2 nor the offset. Though, worth mentioning is that the number of lesions where these calculations could be performed were very few, only eight. This was because many of the areas that were thought to be normal turned out not to be, when analyzed by the pathologist.

Some variations in the measurements might be due to the fullness of the bladder. Cells in the transitional epithelium have an altered shape when the bladder is distended.[23] This is expected to affect the scattering properties of the tissue. Though, examining urologist can control this, and for future investigations more care will be taken to ensure that it does not vary greatly.

4.5 Conclusions

In this study several different parameters have been investigated to differentiate malignant from non-malignant tissue using diffuse reflectance. Some of the parameters, such as the offset, the S650 and the slope of the line fitted to the wavelength region where the blood absorption is negligible, are mostly due to the scattering properties of the tissue. Other parameters such as the concentration of Hb and HbO_2, the apparent absorbance around 515 nm, the total concentration of blood and the O_2-saturation are after correction for scattering mostly due to absorbance. Only the total concentration of blood showed a good demarcation between malignant and non-malignant tissue. The similar concentration of blood in early malignant lesions and in inflammatory tissue makes it difficult to discriminate these two types of lesions, though this method showed a high sensitivity for separating malignant, including dysplastic, from non-malignant regions, 91%.

A1 Basic Bladder Anatomy

A1.1 Anatomy of the Human Bladder

The bladder wall consists of several different layers of tissue, see figure A1.1. Closest to the bladder cavity there is a thin epithelium, the urothelium. This layer consists of transitional cells and is very flexible and allows the volume expansion needed in the bladder. Distending the bladder causes the transitional cells to flatten and the thickness of the urothelium decreases from typically 5-8 cell layers (~ 50 μm) down to 3 or 4, see figure A1.2. During distention, the transitional cells never lose contact with their neighboring cells but regroup into a squamous epithelium. All of the transitional cells are connected to the lamina propria by an ultramicroscopic non-fibrous basement membrane (0.1 μm thick).

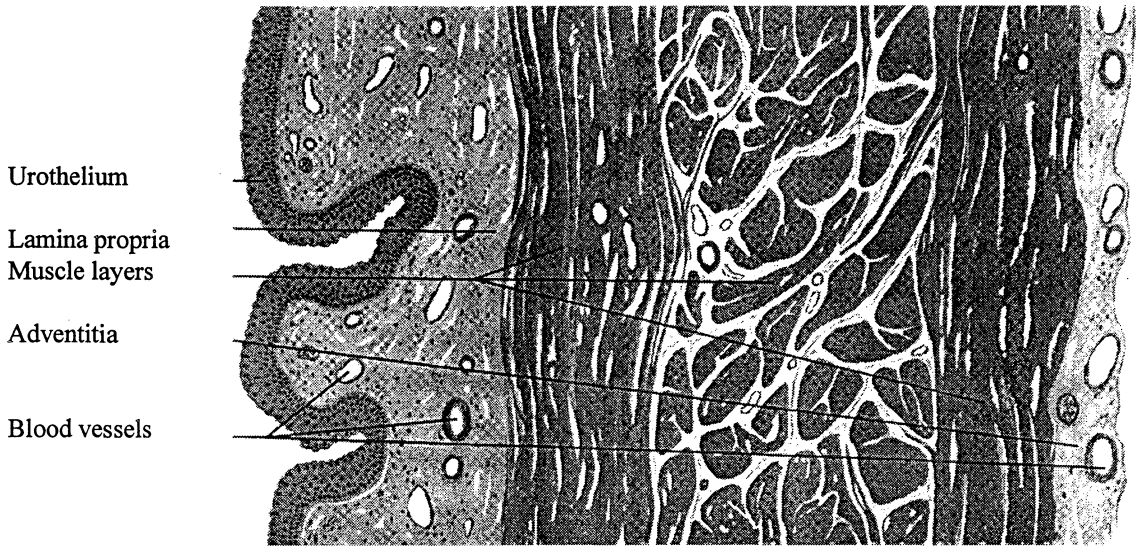

Figure A1.1. Cross section of the bladder wall (extract from drawing by F.H. Netter[1]).

The lamina propria component of the vesical mucosa is composed of collagenous and elastic fibers and fibroblasts. In the lower part of the lamina propria, close to the muscular layers, the connective tissue fibers become looser and this region is sometimes referred to as the submucosa. The lamina propria is the most superficial tissue layer that contains blood vessels. This is important when the invasiveness of a tumor is discussed.

The three interconnected muscular layers form the bulk of the bladder wall. They add strength to the tissue wall and provide the important ability to contract and empty the bladder when it is filled. The bladder muscles consist of smooth muscle cells, which means that the muscles do not need a skeletal structure to be able to contract; they are autonomous. The adventitia, including the fatty tissue is the outermost connective tissue covering of an organ. It is not an integrated part of the organ but is derived from surrounding connective tissue.

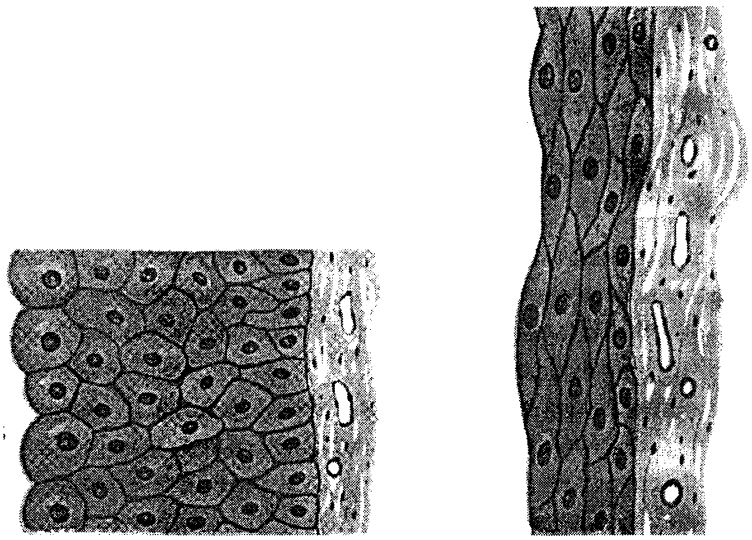

Figure A1.2. Transitional cells in relaxed and distended bladder (extract from drawing by F.H. Netter[1]).

Because of the fact that there is a natural part of entry into the bladder through the urethra, the diagnostic and treatment procedures can be performed using endoscopic techniques. This possibility decreases the number of complications of the procedure and the complexity of the procedure compared to open surgery. The diameter of the urethra is the limiting factor for the dimensions of the equipment that can be used in such a procedure. Fortunately, the tissue in the urethra is rather elastic and relatively large cystoscopes, approximately 10-15 mm in diameter, can be used providing the patient is under an anaesthetic.

A2 Cancer Terminology

A2.1 Introduction

The term "cancer" is used for over 100 forms of malignant diseases. Almost every tissue in the body can produce one or, in some cases, several types of malignancies with its own unique features. There are, however, some basic processes, such as uncontrolled growth and the ability to metastasize (send tumor cells to other organs) that separate malignant cells from normal cells. It has taken almost two decades of research to get a fairly clear and detailed picture of how a malignancy arises and spreads.

A malignant tumor arises from one single cell which over a long period of time, usually decades, has accumulated the required number of mutations (at least half a dozen) in some specific classes of genes to become malignant. There are two main mechanisms that a cell must affect to be able to start a tumor. The first is that the signal pathway that triggers cell division is in some way overstimulated. A mutation in one of the components that controls the growth signal factors will cause a hyper-activated cell proliferation. To become malignant, the cells must also find a way to evade the inhibitory substances the neighboring cells secrete. In a normal cell these substances would stop the cell division and leave the cell in the resting phase, but in the malignant cell the proliferation continues beyond control. Normally the body has control systems which kill abnormal cells, preventing the formation of tumors. If the DNA in a cell is mutated to a certain degree or if other essential systems are damaged, the normal cells will commit suicide via a process called apoptosis. Malignant cells however have developed strategies to avoid this defense mechanism and survive.

A very dangerous situation arises when the malignant tumor has grown so much that it comes in contact with the blood and lymphatic vessels. Because cancer cells can penetrate membranes, the tumor has the opportunity to send some of its cells into the blood stream or the lymphatic drainage. This is a very serious condition and is the start of a process that in many cases is lethal, metastasis.

Most cells are assigned to a certain position in the body (exceptions are e.g. blood cells). To control this localization, each cell has specific adhesion molecules that describe the "area code" for the cell and correspond to receptors in the extracellular matrix (basement membrane). Normally this prevents foreign cells from attaching organs but malignant cells do not obey this addressing system; the reasons for this are not yet fully understood. Although perhaps only one in 10,000 cancer cells that escape the primary tumor survives, one cell is enough to start a secondary tumor.

Metastases cause secondary tumors in a variety of organs, such as in the lungs, liver, kidney, brain and bone marrow. The tumor exfoliates cells into the lymphatic vessels or into the blood stream from where they can travel throughout the body. At this stage the disease may be widely spread and demands systemic treatment, such as chemotherapy, since surgery no longer is curative.

Metastases via the lymphatic system are correlated with the location of the primary tumor. Malignant melanoma often spreads to the lungs, colorectal cancer often to liver etc. because specific lymph nodes are associated with each organ. To detect if a tumor has set metastases through the lymphatic vessels, the lymph nodes must be examined histologically. If there are malignant tumor cells in a lymph node it is said to be

positive and the disease is systemic with a high probability of secondary tumors. At this stage the disease must be treated systemically.

Over 90% of all malignant tumors in the bladder are transitional cell carcinomata and the other histological cell types, in decreasing order of frequency, are squamous cell carcinoma, adenocarcinoma, undifferentiated carcinoma, rhabdomyosarcoma and others.[2]

A2.2 Classification of Urinary Bladder Carcinoma

A2.2.1 Staging

Malignant bladder tumors are classified by how deeply they have penetrated the different cell layers, see figure A2.1. The most superficial tumor, carcinoma *in situ* (Cis) is usually very flat and does not form a tree like papillary structures. In the bladder Cis is located within the urothelium and has not yet penetrated the basement membrane. This type of malignancy is very difficult to detect at an early stage and by the time the tumor is visible it usually has become large and dangerous. In the late stages of Cis, the tumor easily exfoliates, i.e. the tumor cells leave the urothelium and are pushed off into the bladder cavity. The exfoliated cells can readily be detected in a urine sample, but the Cis tumor itself can be more difficult to find during the cystoscopic examination.

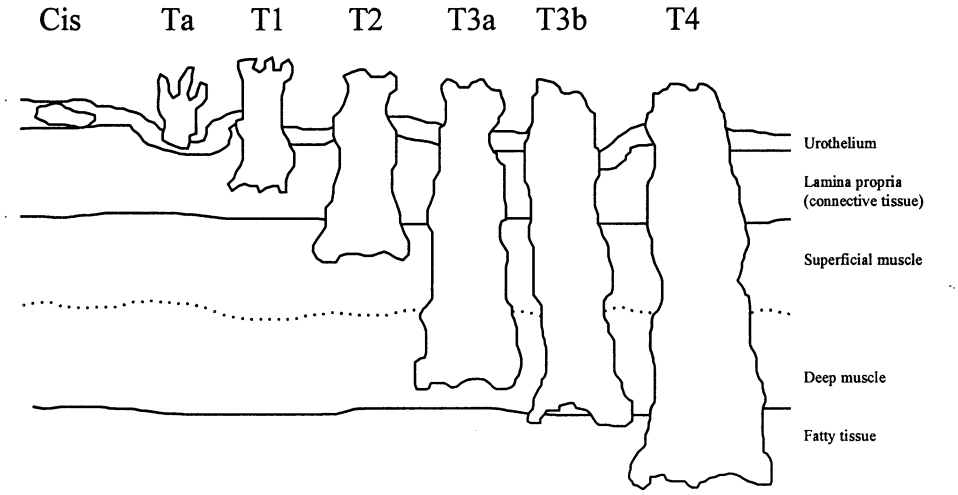

Figure A2.1. Staging of tumors.

When a malignant tumor has penetrated the urothelium but still not the basement membrane it is called Ta. Tumors that have penetrated the basement membrane but not into the muscle are classified as T1. Since the lamina propria contains blood vessels, T1 and all other types of tumors that have penetrated deeper are able to induce metastases and are therefore considered to be invasive. The stage T2 is assigned to malignancies that have started to invade the upper superficial part of the muscle tissue. Tumors that have grown into the deeper muscle layers are called T3a. T3b tumors have penetrated the muscle and grown into the fatty tissue and T4 tumors are so large they have grown through the fat and into other organs.

A2.2.2 Cellular Grading

Histologically the malignant cells are different to normal cells in a number of ways. There are several features the pathologist looks for when determining the grade of a tumor. Some of these features are the polarization of the cells (the cells in normal urothelium are columnar), the nuclear crowding, nuclear border irregularity, increased nuclear size and the chromatin structure. The definition of these features are described in table A2.1. Other features that can provide information are the grade of mitosis, the state of the connective tissue and the cytoplasm.[3]

The grading (G1-G3) is a measurement of the differentiation of the malignant tumor cells compared to normal cells described by the guidelines of UICC 1987.[4]

GX not able to classify the grade

G1 the tumor cells are well differentiated (i.e. highly specialized)

G2 fairly well differentiated

G3 poorly differentiated

G4 undifferentiated, anaplastic

What is important is hence not only the staging of a tumor, but also the grade. The cells in a Cis or TaG3 tumor e.g. are so differentiated that the tumor is most likely to become invasive. The cells in a lesion with mild dysplasia (D1) are identical to those of a G1 tumor. The only difference between these lesions is the staging; the dysplastic lesions are usually more flat. In the same way, cells from a lesion with moderate dysplasia (D2) are identical to G2 tumor cells and cells from severe dysplasia (D3) identical to G3 tumor cells.

Urothelial thickening	Eight or more nuclear layers present in areas sectioned perpendicular to the basal lamina are considered to be abnormal.
Polarization	A. Normal: The basal cells are columnar and arranged perpendicular to the basal layer or the surface. B. Altered: The nuclei no longer have their long axis arranged perpendicular to the basal layer or the surface. The disorientation varies with the degree of the lesion.
Nuclear crowding	A focal increase of nuclei per unit space. This probably reflects the increase in the nuclear-cytoplasmic ratio.
Nuclear border irregularity	Generally, more severe lesions have more irregular nuclei.
Increased nuclear size	Nuclei larger than those of normal intermediate cells. There is normally some variation in nuclear size and shape among cells.
Chromatin	The evaluation of the chromatin structure is very subjective but some guidelines are: A. Normal: Very finely granular (dusty) with a tendency towards peripheral concentration. B. Abnormal: The granules are more distinct and for more severe lesions, the chromatin tends to cluster and is more irregularly distributed throughout the nuclei.

Table A2.1. Guidelines for interpretation of urothelial lesions.[3]

A3 System Response

A3.1 System Response Measurement

All optical components distort the true signal on its way through the system. The spectral transmittance is not uniform and the measured signal (the raw data) has to be corrected by this system response in order to obtain undistorted fluorescence spectra. It is mainly the spectral response of the silicon detector that alters the signal. By taking a spectrum from a source that has a well known intensity distribution and comparing it with the measured spectrum, it is possible to determine the system response of the equipment. Because the optical properties of the system will vary with every single component in the system, it is important to measure the system response curve using exactly the same setup as is used for the *in vivo* measurements.

A3.1.1 Equipment and Results

As a reference light source a standard calibration lamp (1000 W quartz-halogen, model 200A, Optronics Laboratories Inc, Orlando, FL.) was used. The exposure time was set to 150 ms and the temperature of the detector was 15°C - the detector was slightly cooled to minimize the noise. A longer exposure time gives a higher signal at every diode in the array and this gives a better signal-to-noise ratio. However, if the time is too long the detector will be saturated. To make sure that only light coming directly from the calibration lamp would reach the detector the input fiber was wrapped in black cloth, a tunnel of cloth was placed between the lamp and the detector and the light in the room was turned off, see figure A3.1.

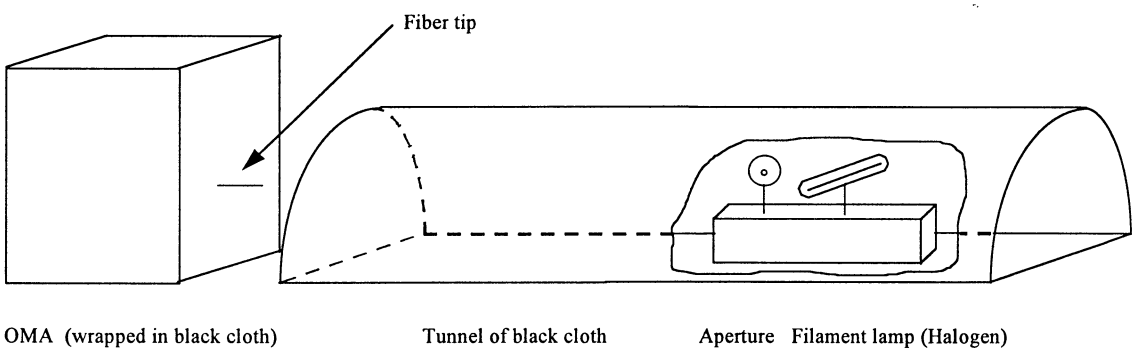

Figure A3.1. System response measurement setup.

A background spectrum was measured by blocking the end of the fiber with a black cap. Subtracting the background spectrum from the calibration lamp spectrum eliminates the effect of possible leakage into the OMA and only the light entering from the fiber end will be significant. The subtraction also corrects for the residual dark current signal generated in the detector, which is not totally eliminated by the cooling.

Because the spectral data of the lamp from the manufacturer was given in 5 nm steps and the OMA spectrometer gave the spectrum in 0.6 nm steps, it was necessary to interpolate the lamp curve to be able to use it directly with the spectrum measured with the system. Since it was known that the intensity spectrum of the lamp was similar to that of a black body radiator, it was fitted to a curve described by Planck's radiation law

$$y(\lambda) = \frac{A}{\lambda^4}\left(\frac{1}{e^{hc/\lambda kT} - 1}\right)$$

by varying the temperature T and the constant A.

The best over all fit of the calibration curve was obtained using A=1.5*10^{14} and T=3650 K and these are the values used, see figure A3.2. The dotted line represents the lamp response given by the manufacturer and the solid line is the fitted blackbody curve. To get a better fit for wavelengths between 200 and 600 nm the values A=2.05*10^{14} and T=3450 K could be used.

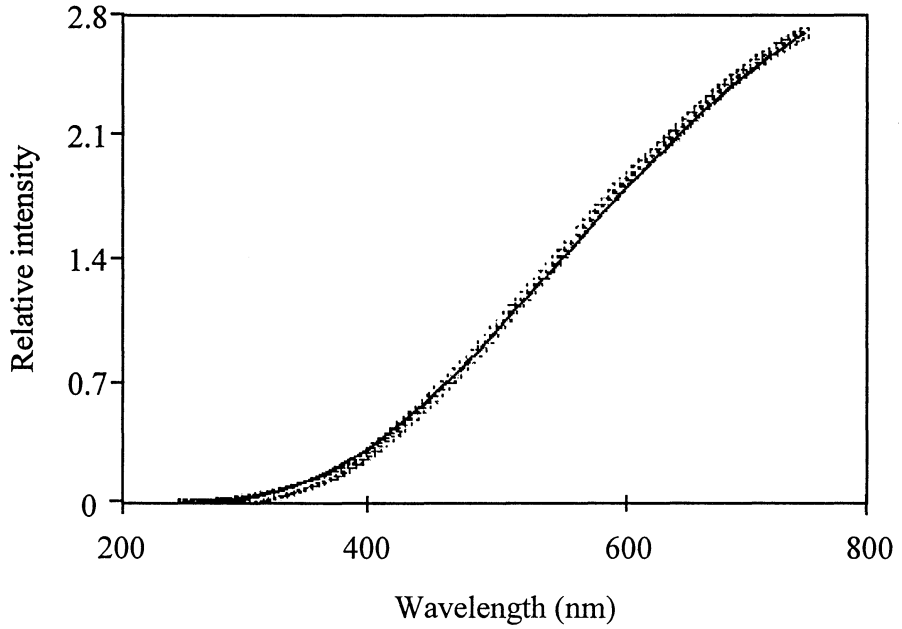

Figure A3.2. Blackbody curve fitted to the data of the calibration lamp.

To get the system response, the fitted blackbody curve was divided by the measured spectrum of the lamp.

$$\text{System response} = \frac{\text{Fitted blackbody curve}}{\text{Measured calibration lamp spectrum}}$$

Every measured spectrum was than divided by this system response.

The system response is a function of the spectral sensitivity of the silicon diode array, the blaze wavelength of the grating and the spectral transmission of the optical components used in the setup. The 450 nm blaze is seen as a maximum in the system response curve in figure A3.3.

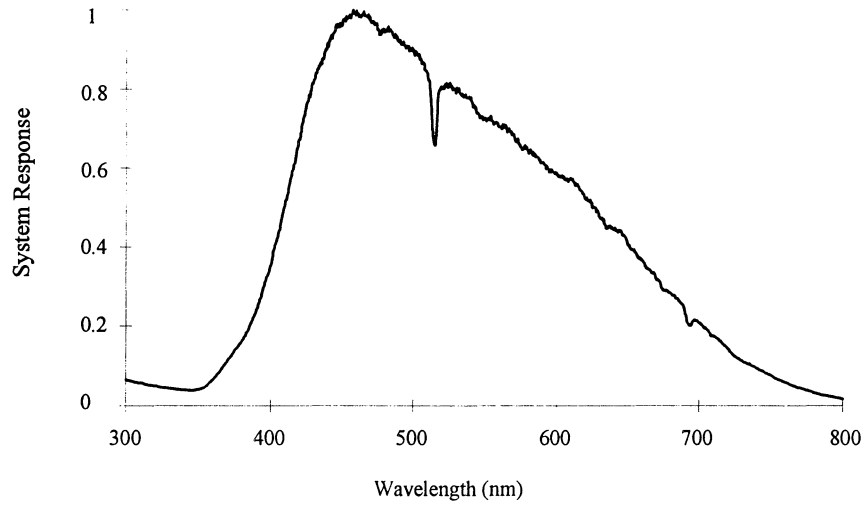

Figure A3.3. System response curve.

A3.1.2 Comments

In the final system response curve there is a dip at 514 nm. This dip is probably the result of someone having used the OMA-system to measure an Ar^+-laser directly and by doing so having damaged the diode array at this wavelength.

A4 Statistical Calculations

A4.1 Introduction

To illustrate how the sensitivity, specificity and the positive and negative predictive values for the different methods were calculated, an example will be given. Say that 32 areas were found to be suspicious (malignant or dysplastic) and 38 not suspicious by the urologist during the cystoscopy. Pathological results later showed that out of the 32 suspicious areas, 27 were positive (true positive) and 5 negative (false positive). For the 38 negative areas, it turned out that 35 were negative (true negative) and 3 positive (false negative). These results are illustrated in table A4.1.

	Positive macroscopic findings	Negative macroscopic findings
Positive pathological results	27	3
Negative pathological results	5	35

Table A4.1. Macroscopic findings and pathological results to illustrate how sensitivity, specificity and positive and negative predictive values for the different methods were calculated.

A4.1.1 Sensitivity

The sensitivity is the proportion of individuals with positive test results for the disease that the test is intended to reveal, i.e. true positive results as a proportion of the total of true positive and false negative results.

Example:

$$sensitivity = \frac{27}{27+3} = 0.9$$

A4.1.2 Specificity

The specificity is the proportion of individuals with negative test results for the disease that the test is intended to reveal, i.e. true negative results as a proportion of the total of true negative and false positive results.

Example:

$$specificity = \frac{35}{35+5} = 0.88$$

A4.1.3 Positive Predictive Value

The positive predictive value is the probability that the area is malignant if the test gives a positive result.

Example:

$$pos.pred.value = \frac{27}{27+5} = 0.84$$

A4.1.4 Negative Predictive Value

The negative predictive value is the probability that the area is not malignant if the test gives a negative result.

Example:

$$neg.pred.value = \frac{35}{35+3} = 0.92$$

Acknowledgments

Doing the work for this thesis at Wellman Laboratories of Photomedicine, Massachusetts General Hospital (MGH), Harvard Medical School in Boston, USA, has truly been a great experience and a perfect way for us to finish our studies. We would very much like to express our sincere gratitude to everybody who has helped us during the work and made our stay in Boston to a very pleasant and joyful time. First of all we would like to thank Frank Koenig, M.D., at Wellman Laboratories together with whom all the work has been carried out. Without Frank our impression of Boston would have been completely different! We would also like to thank our supervisor at Wellman Laboratories, Thomas F. Deutsch, Ph.D, who was always very helpful and supportive. Two persons who also helped us a lot and came up with many good suggestions were Kevin T. Schomacker, Ph.D, and Nikiforos Kollias, Ph.D, also at Wellman Laboratories. At the Department of Urology at MGH we would especially like to thank Alex F. Althausen, M.D., and Francis J. McGovern, M.D., together with whom most of the operations were performed. Very important for this work have also the staff at Wellman Laboratories and the staff at the Department of Urology at MGH been. Finally we would like to thank Stefan Andersson-Engels, Ph.D., who has been our supervisor at the Medical Laser Centre at Lund University and without whom this trip to the USA never would have happened in the first place.

Henrik and Rickard

Lund, June 1997

References

Chapter 2

2.1 Kittrell, Willet, R.L., de los Santos-Pacheo, C., Ratcliff, N.B., Kramer, J.R., Malk, E.G. and Feld, M.S.: *Diagnosis of fibrous arterial atherosclerosis using fluorescence.* Appl. Optics **24/15**: 2280-2281, 1985.

2.2 Baraga, J.J., Rava, R.P., Taroni, P., Kittrel, C., Fitzmaurice, M. and Feld, M.S.: *Laser induced fluorescence of normal and atherosclerotic human aorta using 306-310 nm excitation.* Lasers Surg. Med., **10:** 245, 1990.

2.3 Andersson, P.S., Gustavsson, A., Stenram, U., Svanberg, K. and Svanberg, S.: *Diagnosis of arterial atherosclerosis using laser induced fluorescence.* Lasers Surg. Med. **2;**261, 1987.

2.4 Deckelbaum, L.I., Sarembock, I.J., Stetz, O'Brien, K.M. Cutruzzola, F.W., Gmitro, A.F. and Ezekowitz, M.D.: *In vivo fluorescence spectroscopy of normal and atherosclerotic arteries.* SPIE **906**: 314-319, 1988.

2.5 Crilly, R.J., Gunther, S., Motamedi, M., Berguer, R. and Spears, J.R.: *Fluorescence spectra of normal and atherosclerotic human aorta: Optimum discriminant analysis.* Optical Fibers in Medicin IV, Abraham Katzir (editor), Proc. SPIE **1067**: 110-119, 1989.

2.6 Gaffney, E.J., Clarke, R.H., Lucas, A.R. and Isner, J.M.: *Correlation of fluorescence emission with the plaque content and intimal thickness of atherosclerotic coronary arteries.* Lasers Surg. Med. **9**: 215-228, 1989.

2.7 Richards-Kortum, R., Rava, R.P., Cothren, R., Metha, A., Fitzmaurice, M., Ratliff, N.B., Kramer, J.R., Kittrell, C. and Feld, M.S.: *A model for extraction of diagnostic information from laser induced fluorescence spectra of human artery wall.* Spectrochim. Acta **45A**: 87-93, 1989.

2.8 Andersson-Engels, S., Johansson, J., Stenram, U., Svanberg, K. and Svanberg, S.: *Malignant tumor and atherosclerotic plaque diagnosis using laser induced fluorescence.* IEEE J. Quantum Electron. **12:** 2207-2217, 1990.

2.9 Sartori, M., Sauerbrey, R., Kubodera, S., Tittel, F.K., Roberts, R. and Henry, P.D.: *Autofluorescence maps of atherosclerotic human arteries-a new technique in medical imaging.* IEEE J. Quantum Electron. QE-**23**:1794-1797, 1987.

2.10 Morguet, A., Korber, B., Abel, B., Hippler, H., Wiegand, V and Kreuzer, H.: *Autofluorescence spectroscopy using a XeCl excimer laser system for simultaneous plaque ablation and fluorescence excitation.* Lasers Surg. Med. **14**: 238-248, 1994.

2.11 Bartorelli, A.L., Leon, M.B., Almagor, Y., Prevosti, L.G., Swain, J.A., McIntosh, C.L., Neville, R.F., House, M.D. and Bonner, R.F.: *In vivo atherosclerotic plaque recognition by laser excited fluorescence spectroscopy.* J. Am. Cardiol. **17:** 60B-68B, 1991.

2.12 Geschwind, H.J., Dubois-Rande, J-L, Shafton, E., Buossignac, G. and Wexman, M.: *Percutaneous pulsed laser-assisted balloon angioplasty guided by spectroscopy.* Am. Heart J. **117**: 1147-1152, 1989.

2.13 Leon, M.B., Almagor, Y., Bartorelli, A.L., Prevosti, L.G., Teirstein, P.S., Chang, R., Miller, D.L., Smith, P.D. and Bonner, R.F.: *Fluorescence guided laser*

assisted balloon angioplasty in patients with femoropopliteal occlusions. Circulation **81**: 143-155, 1990.

2.14 Geschwind, H.J., Aptecar, E., Buossignac, G. Dubois-Rande, J-L, Zelinsk, R., Poirot, G. and Tomaru, T.: *Results and follow-up after percutaneous pulsed laser-assisted balloon angioplasty guided by spectroscopy.* Circulation **83**: 787 796, 1991.

2.15 Douek, P.C., Leon, M.B., Geschwind, H.J., Cook, P.S., Selzer, P., Miller, D.L. and Bonner, R.F.: *Occlusive peripheral vascular disease: A multicenter trial of fluorescence guided, pulsed dye laser assisted balloon angioplasty.* Radiology **180**: 127-133, 1991.

2.16 O'Brien K.M., Gmitro, A.F., Gindi, G.R., Stetz, M.L., Cutruzzola, F.W., Laifer, L.I. and Deckelbaum, L.I.: *Development and evaluation of spectral classification algorithms for fluorescence guided angioplasty.* IEEE Trans Biomed Eng **36**: 424-431, 1989.

2.17 Deckelbaum, L.I., Stetz, M.L., O'Brien, K.M., Cutruzzola, F.W., Laifer, L.I. and Gindi, G.R.: *Fluorescence spectroscopy guidance of laser ablation of atherosclerotic plaque.* Lasers Surg. Med. **9**: 205-214, 1989.

2.18 Garrand, T.J., Stetz, M.L., O'Brien, K.M., Gindi, G.R., Sumpio, B.E. and Deckelbaum, L.I.: *Design and evaluation of a fiber optic fluorescence guided laser recanalization system.* Laser Surg. Med. **11**: 106-116, 1991.

2.19 Laufer, G., Wollenek, G., Ruckle, B., Buchelt, M., Kuckla, C., Ruatti, H., Buxbaum, P., Fasol, R. and Zilla, P.: *Characteristics of 308 nm activated photoemission under ablative and non-ablative conditions.* Lasers Surg. Med. **9**: 556-571, 1989.

2.20 Gindi G.R., Darken, C.J., O'Brien, K.M., Stetz, M.L. and Deckelbaum, L.I.: *Neural network and conventional classifiers for fluorescence guided laser angioplasty.* IEEE Trans. Biomed. Eng. **38**: 246-252, 1991.

2.21 Cutruzzola, F.W., Stetz, M.L., O'Brien, K.M., Gindi G.R., Laifer, L.I. Garrand, T.J. and Deckelbaum, L.I.: *Change in laser induced arterial fluorescence during ablation of atherosclerotic plaque.* Lasers Surg. Med. **9**: 109-116, 1989.

2.22 Alfano, R.R., Tang, G.C., Pradham, A., Lam, W., Choy, D.S. and Opher, E.: *Fluorescence spectra from cancerous and normal human breast and lung tissues.* IEEE J. Quantum Electron. QE-**23**:1806-1811,1987.

2.23 Sundström, F., Fredriksson, K., Montan, S., Hafström-Björkman, U. and Ström, J.: *Laser induced fluorescence from sound and carious tooth substance: Spectroscopic studies.* Swed. Dent. J. **9**: 71, 1985.

2.24 Alfano, R.R., Lam, W., Zarrabi, H., Alfano, M.A., Cordero, J., D.B. and Swenberg, C.E.: *Human teeth with and without caries studied by laser scattering fluorescence and absorption spectroscopy.* IEEE J. Quantum Electron. QE-**20**: 1512-1516, 1984.

2.25 Andersson-Engels, S., Elner, Å., Johansson, J., Karlson, S-E, Salford, L.G., Strömblad, L-G, Svanberg, K. and Svanberg, S. *Clinical recording of laser induced fluorescence spectra for evaluation of tumor demarcation feasibility in selected clinical specialities.* Lasers Med. Sci. **6**: 415-424, 1991.

2.26 Andersson, P.S., Kjellen, E., Montan, S., Svanberg, K. and Svanberg, S.: *Autofluorescence of various rodent tissues and human skin tumor samples.* Lasers Med Sci. **2**:41-49, 1987.

2.27 Mahadevan, A., Follen-Mitchell, M., Silva, E., Thomsen, S. and Richards-Kortum, R.: *Study of the fluorescence properties of normal and neoplastic human cervical tissue.* Lasers Surg. Med. **13**: 647-655, 1993.

2.28 Richards-Kortum, R., Tong, L., Rava, R., Fitzmaurice, M., Petras, R., Sivac, M. and Feld, M.S.: *Spectral studies of GI tissues: optimizing excitation and emission wavelengths for discrimination of normal and adenomatous tissues* (abstr.) Lasers Surg. Med. **35**: 184, 1989.

2.29 Yakshe, P.N., Bonner, R.F., Cohen, P., Leon, M.B. and Fleischer, D.E.: *Laser induced fluorescence spectroscopy may distinguish colon cancer from normal colon* (abstr.) Gastrointest. Endosc. **35**:184, 1989.

2.30 Cothren, R.M., Richards-Kortum, R., Sivac, M.V. Jr, Fitzmaurice, M., Rava, R.P., Boyce, G.A., Doxtader, M., Blackman, R., Ivanc, T.B., Hayes, G.B., Feld, M.S. and Petras, R.E.: *Gastrointestinal tissue diagnostics by laser induced fluorescence spectroscopy at endoscopy.* Gastrointest. Endosc. **36**:1005-111, 1990.

2.31 Rava, R., Richards-Kortum, R., Fitzmaurice, M., Cothren, R., Petras, R., Sivak, M., Levin, H. and Feld, M.S.: *Early detection of dysplasia in colon and bladder tissue using laser induced fluorescence.* SPIE Vol. 1426 Optical methods for tumor treatment and early diagnosis: Mechanisms and techniques. 1991.

2.32 Schomacker, K.T., Frisoli, J.K., Compton, C.C., Flotte, T.J., Richter, J.M., Nishioka, N.S. and Deutsch, T.F.: *Ultraviolet laser-induced fluorescence of colonic tissue: basic biology and diagnostic potential.* Lasers Surg. Med., **12**: 63, 1992.

2.33 Kapadia, C.R., Cutruzzola, F.W., O'Brien, K.M., Stetz, M.L., Enriquez, R. and Deckelbaum, L.I.: *Laser-induced fluorescence spectroscopy on human colonic mucosa.* Gastroenterology, **99**: 150-157, 1990.

2.34 Koenig, F., McGovern, F.J., Althausen, A.F., Deutsch, T.H. and Schomacker, K.T.: *Laser induced autofluorescence diagnosis of bladder cancer.* J. Urol., **156**: 1597, 1996.

2.35 Anidjar, M., Ettori, D., Cussenot, O., Meria, P., Desgrandchamps, F., Cortesse, A., Teillac, P., Le Duc, A. and Avrillier, S.: *Laser induced autofluorescence diagnosis of bladder tumors: Dependence on the excitation wavelength.* J. Urol., **156**: 1590, 1996.

2.36 Rokahr, I., Andersson-Engels, S., Svanberg, S., D'Hallewin, M.A., Baert, L., Wang and Svanberg, K.: *Optical detection of human urinary bladder carcinoma utilizing tissue autofluorescence and protoporphyrin IX-induced fluorescence following low-dose ALA instillation.* Proceeding BiOS'95, Barcelona, sept 9-13, 1995.

2.37 Baert, L., Berg, R., Van Damme, B., D'Hallewin, M.A., Johansson, J., Svanberg, K. and Svanberg, S.: *Clinical fluorescence diagnosis of human bladder carcinoma following low-dose Photofrin injection.* Urology, **41**: 322, 1993.

2.38 D'Hallewin, M.A., Baert, L. and Vanherzeele, H.: *Fluorescence imaging of bladder cancer.* Acta Uro. Belg., **62**: 49, 1994.

2.39 Schomacker, K.T., Flotte, T.J. and Deutsch, T.F.: *Detection of chemically-induced dysplasia in rat urinary bladder with laser-induced fluorescence.* In: Advances in Laser and Light Spectroscopy to Diagnose Cancer and Other Diseases. Edited by R.R. Alfano. Proc. SPIE **2135**: 76-79, 1994.

2.40 Chance, B., Cohen, P., Jöbsis, F. and Schoener, B.: *Intracellular oxidation-reduction states in vivo.* Science **137**: 499, 1962.

2.41 Svanberg, S.: *Atomic and molecular spectroscopy*. Springer Verlag sec. ed., 1992.
2.42 Daly, J.J.: *Carcinoma in situ of the urothelium.* Urol. Clin. N. Amer. **3**: 87, 1976.
2.43 Wang, T.D., van Dam, J., Crawford, J.M., Preisinger, E.A., Wang, Y. and Feld, M.S.: *Fluorescence endoscopic imaging of human colonic adenomas.* Gastroenterology **111**:1182, 1996.
2.44 Lam, S., MacAulay, C., Hung, J., LeRiche, J., Profio, A.E. and Palcic, B.: *Detection of dysplasia and carcinoma in situ with a lung imaging fluorescence endoscope device*. J. Thoracic Cardiov. Sur. **105(6)**:1035, 1993.
2.45 Svanberg, K., af Klinteberg, C., Nilsson, A., Wang, I., Andersson-Engels, S. and Svanberg, S.: *Laser spectroscopy in tissue characterization.* Biomedical Optical Spectroscopy and Diagnostics, Technical Digest (Optical Society of America, Washington DC), 172-174, 1996.

Chapter 3

3.1 Henderson, B. W. and Dougherty, T. J.: *Review Article: How Does Photodynamic Therapy Work?* Photochem. Photobiol. **55**: 145-157, 1992.
3.2 Lipson, R. L. and Baldes, E. J.: *The Photodynamic Properties of a Particular Hematopotphyrin Derivative.* Arch. Derm. **82**: 76-84, 1960.
3.3 Dougherty, T. J.: *Photoradiation Therapy (PRT) of Malignant Tumors.* CRC Clinical Review in Oncology/Hematology. CRC, New York, 1984.
3.4 Manyak, M. J., Russo, A., Smith, P. D. and Glatstein, E.: *Photodynamic Therapy.* J. Clin. Oncol. **6**: 380-391, 1988.
3.5 Berg, R.: *Laser-Based Cancer Diagnostics and Therapy-Tissue Optics Concideration*s. PhD thesis, Lund Institute of Technology, LRAP-184, 558, 1995.
3.6 Parrish, J.A., Deutsch, T.F.: Laser photomedicine. IEEE J. QE-20, 1386, 1984.
3.7 Hayata, Y., Dougherty, T.J.: Lasers and Hematoporphyrin Derivative in Cancer. (Ikaku-shoin, Tokyo), 1983.
3.8 Andreoni, A. and Cubeddua, C.A.: Porphyrins in Tumor Phototherapy (Plenum, New York), 1984.
3.9 Svanberg, S.: *Medical diagnostics using laser-induced fluorescence*. Phys. Scr. T **17**: 469, 1987.
3.10 Svanberg, S.: *Medical applications of laser spectroscopy.* Phys. Scr. T **26**: 90, 1989.
3.11 Kato, H. and Cortese, D.A.: *Early detection of lung cancer by means of hematoporphyrin derivative fluorescence and laser photoradiation.* Clinics in Chest Medicine **6**: 237, 1985.
3.12 Andersson-Engels, S., Brun, A., Kjellén, E. Salford, L.G., Strömblad, L.G., Svanberg, K. and Svanberg, S.: *Identification of brain tumors in rats using laser-induced fluorescence and haemetoporphyrin derivative*. Laser Med. Sci. **4**: 241, 1989.
3.13 Andersson-Engels, S., Berg, R., Colleen, S., Johansson, J., Karlsson, S.-E., Lundgren, R., Salford, L.G., Stroemblad, L.-G., Svanberg, K. and Svanberg, S.: *In vivo fluorescence spectra of malignant lesions in various clinical specialties.* Photodynamic Therapy and Biomedical Lasers, Spinelli, P., Dal Fante, M. and

Marchesini, R., eds.: 871-875 (Elsevier Science Publishers B.V.Amsterdam, the Netherlands), 1992.

3.14 Kennedy, J.C., Pottier, R.H. and Pross, D.C.: *Photodynamic therapy with endogenous protoporphyrin IX: Basic principles and present clinical experience*, J.Photochem. Photobiol. B:Biol. **6**: 143-148, 1990.

3.15 Iinuma, S., Farshi, S.S., Ortel, B. and Hasan, T.: *A mechanistic study of cellular photodestruction with 5-aminolaevulinic acid-induced porphyrin.* Br. J. Cancer, **70**: 21-28, 1994.

3.16 Bedwell, J., MacRobert, A.J., Phillips, D. and Bown, S.G.: *Fluorescence distribution and photodynamic effect of ALA-induced PpIX in the DMH rat colonic tumor model.* Br. J. Cancer, **65**: 818-824, 1992.

3.17 Peng, Q., Moan, J., Warloe, T., Nesland, J.M. and Rimington, C.: *Distribution and photosensitising efficiency of porphyrins induced by application of exogenous 5-aminolevulinic acid in mice bearing mammary carcinoma.* Int. J. Cancer, **52**: 433-443, 1992.

3.18 Iinuma, S., Bachor, R., Flotte, T. and Hasan, T.: *Biodistribution and phototoxicity of 5-aminolevulinic acid-induced PpIX in an orthotopic rat bladder tumor model.* J. Urol., **153**: 802-806, 1995.

3.19 Grant, W.E., Hopper, C., MacRobert, A.J., Speight, P.M. and Bown, S.G.: *Photodynamic therapy of oral cancer: photosensitisation with systemic aminolevulinic acid.* Lancet **342**: 147-148, 1993.

3.20 Baumgartner, R., Kriegmair, M., Stepp, H.G., Lumper, W., Heil, P., Riesenberg, R., Stocker, S. and Hofstetter, A.G.: *Photodynamic diagnosis following intravesical instillation of aminolevulinic acid (ALA): first clinical experiences in urology.* Proc. SPIE Vol. 1881: 20-25, 1993.

3.21 Kriegmair, M., Baumgartner, R., Knüchel, R., Steinbach, P., Ehsan, A., Lumper, W., Hofstädter, F. and Hofstetter, A.: *Fluorescence photodetection of eoplastic othelial lesions following intravesical instillation of 5-aminolevulinic acid.* Urology, **44**: 836, 1994.

3.22 Kriegmair, M., Baumgartner, R., Knüchel, R., Stepp, H., Hofstädter, F. and Hofstetter, A.: *Detection of early bladder cancer by 5-aminolevulinic acid induced porphyrin fluorescence.* J Urol., **155**: 105-110, 1996.

3.23 Dougherty, T.J.: *Photosensitizers Therapy and Detection of Malignant Tumors.* J. Photochem. Photobiol., **45**: 879-889, 1987.

3.24 Hasan, T. and Parrish, J.A.: *Photodynamic Therapy of Cancer.* In: JF Holland, E. Frei III, Bast Jr R.C., Kufe, D.W., Morton, D.L. and Weichselbaum, R.R. Cancer Medicine, Fourth Edition. Williams & Wilkins, Chapter 50(1), 739-751, 1996.

3.25 Dailey, H.A. and Smith, A.: *Differential interaction of porphyrins used in photoradiation therapy with ferrochelatase.* Biochem. J., **223**: 441-445, 1984.

3.26 Leibovici, L., Schoenfeld, N.I.L.I., Yehoshua, H.A., Mamet, R., Rakowski, E., Shindel, A. and Atsmon, A.: *Activity of porphobilinogen deaminase in peripheral blood mononuclear cells of patients with metastatic cancer.* Cancer, **62**: 2297-2300, 1988.

3.27 Andersson-Engels, S.: *Laser-induced fluorescence for medical diagnostics.* Lund Reports on Atomic Physics, LRAP-108, Lund, Sweden, 1989.

3.28 Campbell, M. J. and Machin, D.: *Probability and decision making: diagnostic tests*. In: medical Statistics, 2nd ed. New York: John Wiley & Sons, vol. 2, chapt. 3.2: 34-35, 1993.
3.29 Soloway, M. S., Murphy, W., Rao, M. K. and Cox, C.: *Serial multiple-site biopsies in patients with bladder cancer.* J.Urol., **120**: 57, 1978.
3.30 Heney, N.M., Ahmed, S., Flanagan, M.J., Frable, W., Corder, M.P., Hafermann, M.D. and Hawkins, I.R. for National Bladder Cancer Collaborative Group A.: *Superficial bladder cancer: progression and recurrence.* J. Urol., **130**: 1083, 1983.
3.31 Flamm, J. and Dona, S.: *The significance of Bladder quadrant biopsies in patients with primary superficial bladder carcinoma.* Eur. Urol., **16**: 81, 1989.
3.32 George, K. N., William, J. F. and William, M. M.: *Pathology Annuals.* Part I: 219-233, 1982.

Chapter 4

4.1 Kollias, N.: *The Physical Basis of Skin Color and Its Evaluation.* Clinics in Dermatology, Elsevier Science Inc., New York, 361-367, 1995.
4.2 Marieb, E.N.: *Tissue: The living fabric.* In:Adams M, Olivier S, eds. "Human Anatomy and Physiology." CA:Benjamin/Cummings, p. 110, 1992.
4.3 Anderson, R.R. and Parish, J.A.: *The optics of human skin.* J. Invest. Dermatol. **77**: 13-19, 1981.
4.4 Edwards, E.A. and Duntley, S.Q.: *The pigments and color of living human skin.* Am. J. Anatomy, **65**: 1-33, 1939.
4.5 Marchesini, R., Brambilla, M., Clemente, C., Maniezzo, M., Sichirollo, A.E., Testori, A., Venturoli, D.R. and Cascinelli, N.: *In vivo spectrophotometric evaluation of neoplastic and non-neoplastic skin pigmented lesions-I. Reflectance measurements*. Photochem. & Photobiol. 53 No. **1**: 77-84, 1991.
4.6 Marchesini, R., Cascinelli, N., Brambilla, M., Clemente, C., Mascheroni, L., Pignoli, E. and Venturoli, D. R.: *In vivo spectrophotomentric evaluation of neoplastic and non-neoplastic skin pigmented lesions-II. Discriminate analysis between nevus and melanoma.* Photochem. & Photobiol. 55 No. **4**: 515-522, 1992.
4.7 Marchesini R., Tomatis, S., Bartoli, C., Bono, A., Clemente, C., Cupeta, C., Del Prato, I., Pignoli, E., Sichirollo, A.E. and Cascinelli, N.: *In vivo spectrophotomentric evaluation of neoplastic and non-neoplastic skin pigmented lesions. III. CCD camera based reflectance imaging*. Photochem. and photobiol. **62** (1): 151-154, 1995.
4.8 Curley, R.K., Cook, M.G., Fallowfield, M.E. and Marsden, R.A.: *Accuracy in clinically evaluating pigmented lesions*. Br. Med. J. **299**:16-18, 1989.
4.9 Wallace, V. P.: *Spectrophotometry for the assessment of pigmented skin lesions.* Biomedical Optical Spectroscopy and Diagnostics. Technical Digest, pp. 67-69, 1996.
4.10 Dawson, J.B., Barker, D.J., Ellis, E., Grassam, J., Cotteril, A., Fischer, G.W. and Feather, J.W.: *A theoretical and experimental study of light absorption and scattering by in vivo skin.* Phys. Med. Biol. **25**: 696-709, 1980.

4.11 Kollias, N. and Baqer, A.: *Spectroscopic characteristics of human skin* in vivo. J. Invest. Dermat. **85**: 38-42, 1985.

4.12 Feather, J.W., Ellis, D.J. and Leslie, G.: *A portable reflectometer for the rapid quantification of cutaneous haemoglobin and melanin.* Phys. Med. Biol. **33**: 711-722, 1988.

4.13 Kollias, N., Gillies, R. Muccini, J.A., Uyeyama, R.K., Phillips, S.B. and Drake, L.A.: *A single parameter, oxygenated hemoglobin, can be used to quantify experimental irritant-induced inflammation.* J. Invest. Dermatology, **104**: 421-424, 1995.

4.14 Knoefel, W.T., Kollias, N., Rattner, D.W., Nishioka, N.S. and Warshaw, A.L.: *Reflectance spectroscopy of pancreatic microcirculation.* J. Applied Physiology, **80** (1): 116-123, 1996.

4.15 Mourant, J.R., Bigio, I.J. Boyer, J., Conn, R.L., Johnson, T. and Shimada, T.: *Spectrocscopic diagnosis of bladder cancer with elastic scattering.* Lasers in Surgery and Medicine, **17**: 350-357, 1995.

4.16 Mourant, J.R., Bigio, I.J., Boyer, J., Johnson, T.M., Lacey, J., Bohorfoush, A.G. and Mellow, M.: *Elastic scattering spectroscopy as a diagnostic tool for differentiating pathologies in the gastrointestinal tract: Preliminary testing.* J. Biomedical Optics, (2): 192-199, 1996.

4.17 Takatani, S., Cheung, P.W. and Ernst, E.A.: *A non-invasive tissue reflectance oximeter. An instrument for measurment of tissue hemoglobin oxygen saturation in vivo.* Ann. Biomed. Eng., **8**: 1-15, 1980.

4.18 Mendelson, Y. and Ochs, B.D.: *Non-invasive pulse oximeter utilizing skin reflectance photoplethysmography.* IEEE Trans. Biomed. Eng. **35**: 798-805, 1988.

4.19 Mourant, J.R. and Hielscher, A.: *The significance of fiber numerical aperture for optical measurements of turbid media.* Biomedical Optical Spectroscopy and Diagnostics. Technical Digest: 132-134, 1996.

4.20 Andersson, P.S., Montán, S. and Svanberg, S.: Multi-spectral system for medical fluorescence imaging. IEEE J. QE-23. 1798, 1987.

4.21 Van Assendelft, O.W.: *Spectrophotometry of Hemoglobin Derivatives*. Assen, The Netherlands: Van Gorcum, 1970.

4.22 Campbell, M.J. and Machin, D.: *Probability and decision making: diagnostic tests*. In: Medical Statistics, 2nd ed. New York: John Wiley & Sons, vol. 2, chapt. 3.2: 34-35, 1993.

4.23 Junqueira, L.C., Carneiro, J and Kelley, R.O.: *Urinary system.* In: "Basic Histology." Appelton and Lange: 391, 1992.

Appendix 1

A1.1. Netter, F.H.: The Ciba Collection of Medical Illustrations, **6**: 24, 1973.

Appendix 2

A2.1 Scientific American, sept. 1996.

A2.2 Ro, J.Y., Staerkel, G.A. and Ayala, A.G.: *Cytologic and histologic features of superficial bladder cancer*. Urol. Clin. North Am. **19**: 435-453, 1992.

A2.3 Nagy, G.K., Frable, W. and Murphy, W.M.: *Classification of pre-malignant urothelial abnormalities: A Delphi study of the national bladder cancer collaborative group A*. Pathology Annals Part I: 219-233, 1982.

A2.4 UICC TNM-Atlas. 2 ed.:245-250. Springer Verlag Berlin, Heidelberg, New York, 1990.